Thermo Electron
CORPORATION

DISCLAIMER

Report No. TE4258/4247-83-80

DOE/JPL
ADVANCED THERMIONIC
TECHNOLOGY PROGRAM

PROGRESS REPORT NO. 40

July-August-September
1979

DOE Contract EY-76-C-02-3056
JPL Contract 955009

Prepared by

Thermo Electron Corporation
101 First Avenue
Waltham, Massachusetts 02154

CONTENTS

2.0 PART TWO: JPL TASKS

DOE Contract No. EY-76-C-02-3056
WORK BREAKDOWN STRUCTURE

7911-11

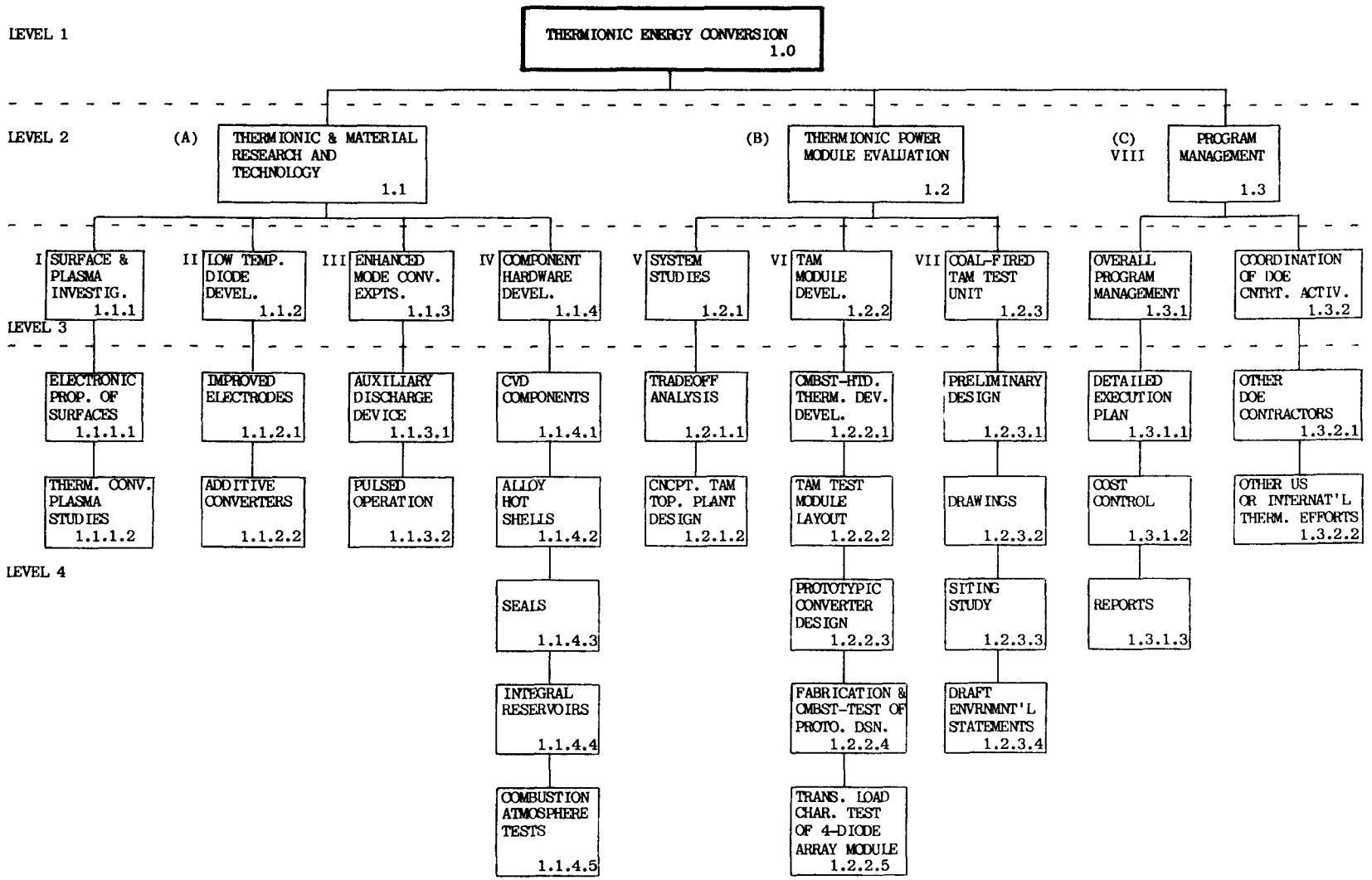

Note: Roman Numerals Designate Level at Which Tasks are to be Reported

JPL CONTRACT NO. 955009
WORK BREAKDOWN STRUCTURE

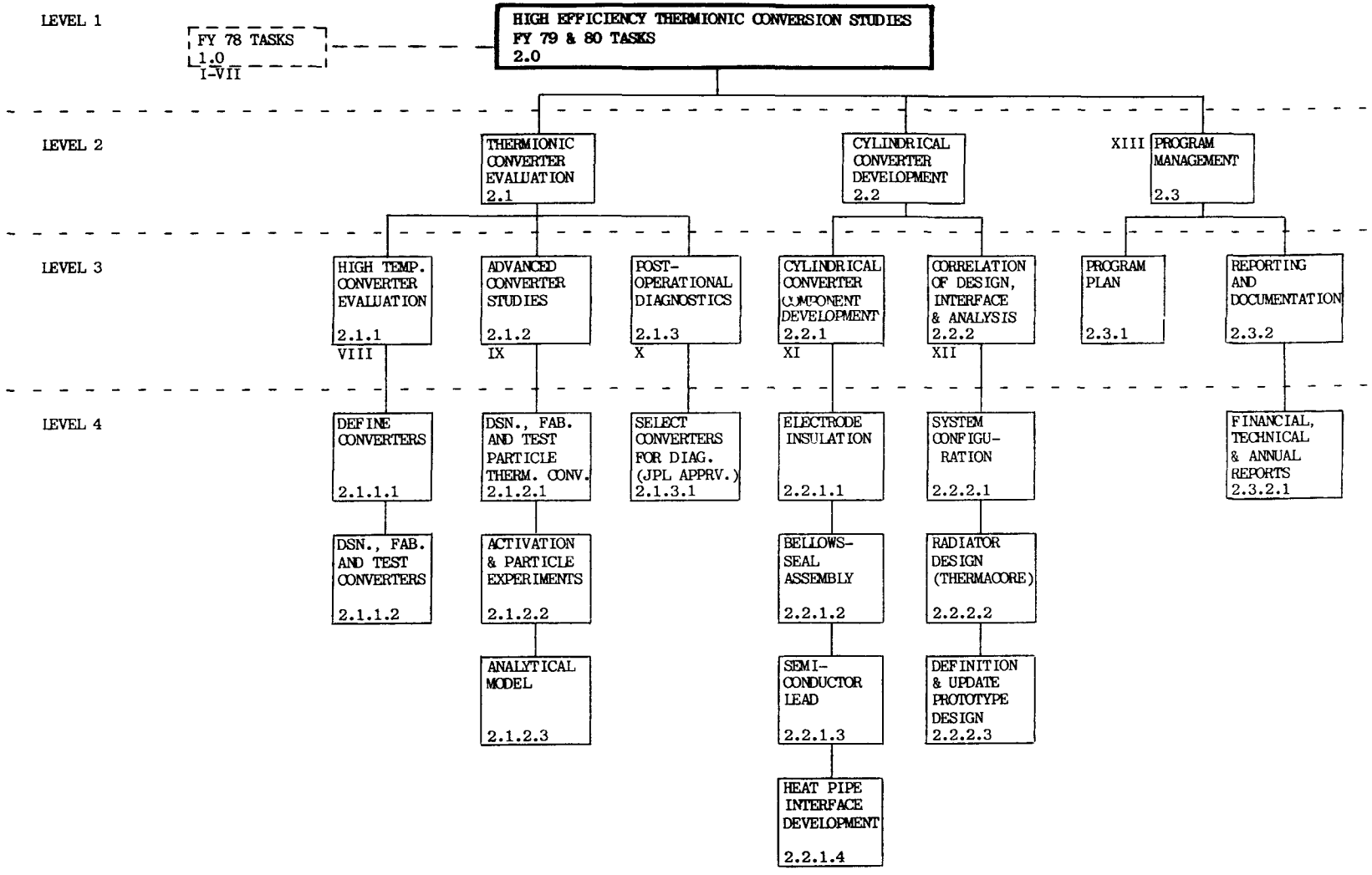

Note. Roman Numerals Designate Level at which Tasks are to be Reported.

INTRODUCTION AND SUMMARY

The Advanced Thermionic Technology Program at Thermo Electron Corporation is sponsored by the Department of Energy (DOE) and the National Aeronautics and Space Administration (NASA) via the Jet Propulsion Laboratory (JPL).

The primary long-term goal of the DOE effort is to improve TEC performance to the level that thermionic topping of fossil fuel steam powerplants becomes technically possible and economically attractive. An intermediate goal is to demonstrate an in-boiler thermionic module in the early 1980's. A short-term goal is the demonstration of the reliability of thermionic operation in a combustion environment.

The focus of the JPL program is to develop thermionic conversion technology appropriate for nuclear electric propulsion (NEP) missions. These missions require operation at collector temperatures substantially higher than those associated with terrestrial applications.

The DOE and JPL tasks for developing thermionic energy conversion (TEC) are complementary and synergistic. Converter performance improvement is an area in which one agency's program supports the effort of the other.

This report covers progress made during the three-month period from July through September 1979. During this period, significant accomplishments include:

DOE PROGRAM

- Demonstration of 2300 hours of stable operation (Silicon Carbide Converter No. 1) in a combustion environment at emitter temperatures at, or above, 1600 K. This test is continuing.
- Fabrication of two leaktight composite CVD (SiC/C/W) hot shell-emitter structures two inches in diameter.
- Reproduction of W(100)/O/Zr emitter work function obtained at the Oregon Graduate Center.
- Formation of an anlytical model of the ignited mode thermionic diode which predicts the operating conditions associated with the onset of a double sheath at the emitter.

JPL PROGRAM

- Demonstration of oxygen enhancement of a molybdenum emitter from a tungsten oxide collector.
- Development of a technique for casting sapphire prototypic of NEP thermionic reactor system design.
- Development of a technique for bonding lanthanum hexaboride to rhenium that was stable for 150 hours at temperatures ranging between 1600 and 1700 K.
- Formulation of an assembly procedure for fabricating thermionic converters on an emitter heat pipe.

1.0 PART ONE: DOE TASKS

1.1 THERMIONIC AND MATERIAL RESEARCH AND TECHNOLOGY

1.1.1 TASK I. SURFACE AND PLASMA INVESTIGATIONS

The objective of this task is to support the development of thermionic energy converters by providing experimental data and analyses relating to plasma characteristics and electrode properties.

A. Surface Characterization Chamber Experiments

An emitter that could provide practical current densitites (e.g., 10 A/cm^2) at projected operating temperatures around 1600 K would be highly desirable. Such an emitter would allow the cesium pressure to be optimized for the collector alone to take advantage of its minimum work function (rather than the cesium pressure being a compromise between the emitter and collector characteristics). In addition, most of the techniques for reducing the voltage losses in the plasma require an emitter that will operate at very low cesium pressure.

An electrode formed by the coadsorption of zirconium (Zr) and oxygen (O) on W(100) is a promising candidate emitter that would not require cesium exposure for practical current densities. In studies at the Oregon Graduate Center, Danielson and Swanson[1] found that adsorption of Zr onto W(100) followed by heating in an oxygen partial pressure produces both rapid diffusion of a Zr-O complex into the bulk, and formation of a tungsten oxide layer. Heating in vacuum desorbs the tungsten oxide and segregates the Zr-O complex to the surface. This Zr-O-W composite surface has a FERP work function of about 2.7 eV. Additional carbon has yielded FERP work functions as low as 2.4 eV.

During the subject reporting period, Danielson has modified the Surface Characterization Chamber (SCC) in order to continue investigation of the Zr-O-W emitter at Thermo Electron. If a stable electrode with a work function as low as 2.6 eV can be demonstrated, it will be evaluated as an emitter in a thermionic converter.

The first step in this effort was to develop a Zr source which would uniformly coat an emitter 0.5 inch in

diameter. This was achieved by evaporating Zr from a ring source. An analytical discussion of ring sources[2] indicates that a sample with a given diameter, D, can be coated uniformly to within ± 5% by a ring source with the same diameter, D, placed 0.65D from the sample (see Figure 1A).

Several ring sources were constructed by wrapping 5-mil Zr wire onto 10-mil W wire. Bell jar experiments showed that the temperature distribution across the ring could be made uniform by splitting the ring into two halves and wrapping the straight sections with 5-mil W wire. The optimized source is shown in Figure 1B. The two sections are heated directly with independent power supplies. The Zr wire is melted onto the W wire prior to evaporation. The maximum temperature difference across the ring at 1900 K is 40 K.

This ring source and a W(100) emitter were mounted in the SCC. The emitter was fabricated at Thermo Electron using chemical vapor deposition of tungsten hexafluoride. Subsequently, it was polished mechanically and electrically.

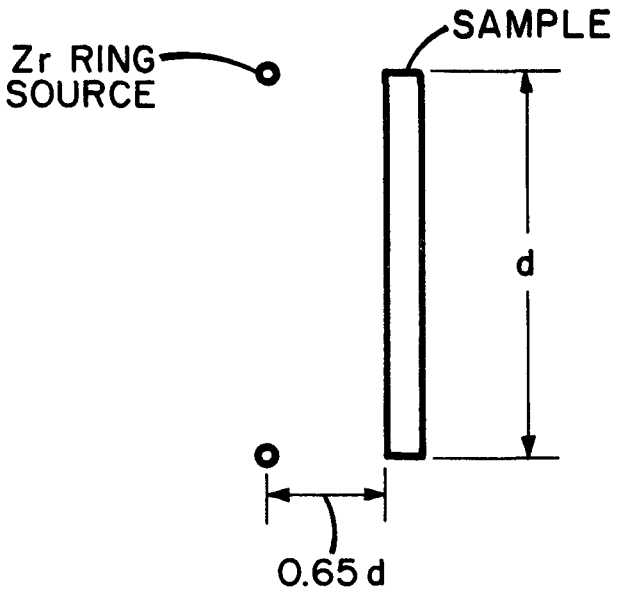

Figure 1A. Mounting Arrangement of Sample and Source

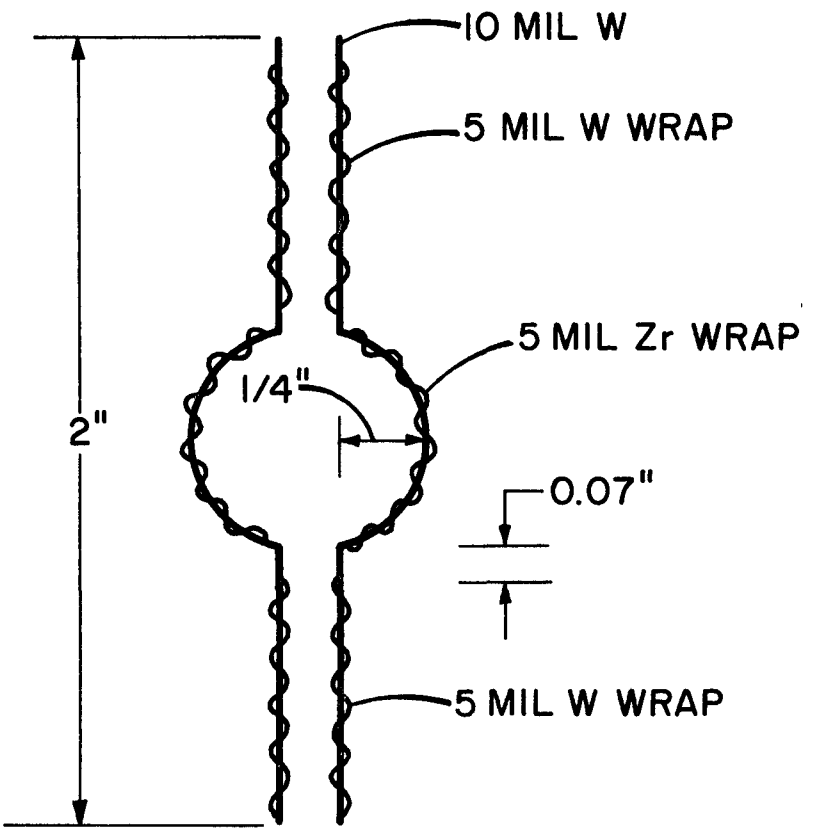

(SHOWN TWICE ACTUAL SIZE)

Figure 1B. Zirconium Source

The orientation of this electrode was confirmed by X-ray diffraction. Zirconium was evaporated onto the emitter, and the Zr distribution as measured by Auger peak-to-peak height is shown in Figure 2. The Zr coverage in both horizontal and vertical directions is constant to within $\pm$ 6%. This uniformity is quite satisfactory and in excellent agreement with the theoretical prediction.

The CVD W(100) emitter was then: (1) alternately dosed with Zr, (2) heated in 1 x 10^{-7} torr O_2 for two minutes at 1500 K, and (3) heated in vacuum for ten seconds at 2000 - 2100 K. These treatments cause diffusion of a Zr/O complex from surface to bulk and back to surface. A summary of work function and percent coverages after the vacuum heating for several runs with the CVD W(100) emitter is given in Table I. The Zr does indeed diffuse into the bulk after the O_2 heating and reappear after the vacuum heating. However, the work functions of 2.9 - 3.0 eV are somewhat higher than those reported in Reference 1. Possible causes for this discrepancy are: (1) the use of CVD W(100) rather than single crystal W(100), (2) the rather large nitrogen coverages caused by outgassing during heating of the

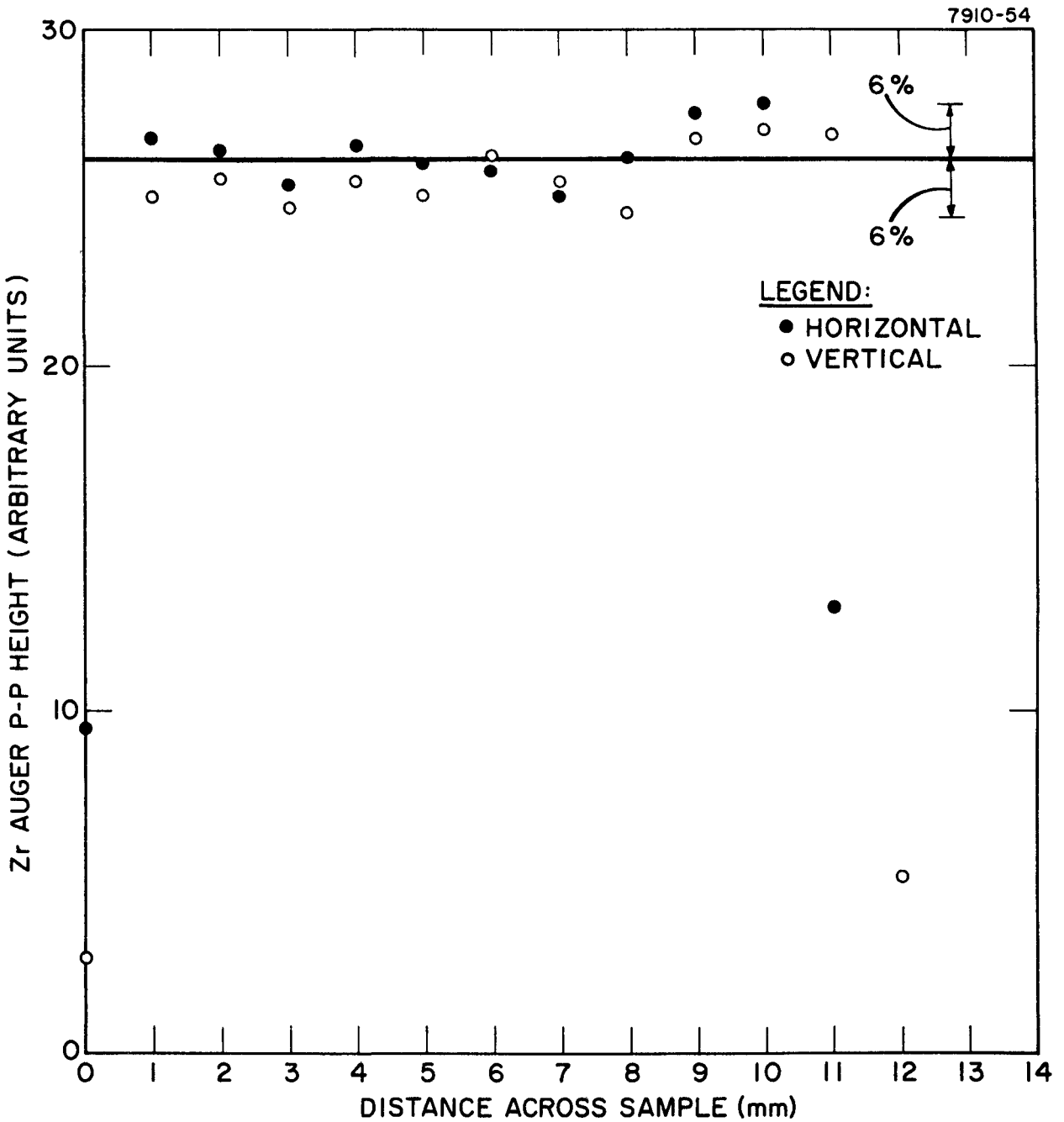

Figure 2. Zirconium Distribution Across CVD W(100)

TABLE I

FERP WORK FUNCTION OF CVD W(100) VERSUS COVERAGE*

WORK FUNCTION (eV)	Zr_{147} (%)	O_{510} (%)	W_{169} (%)	C_{272} (%)	N_{380} (%)
2.88	27	20	40	1	11
2.94	27	14	40	2	16
2.90	26	21	45	-	7
2.93	26	22	43	1	7
2.89	23	18	51	2	5
2.97	27	12	35	3	22
2.99	24	23	47	-	5

*Subscripts on elements denote energy of auger peak used to calculate coverages.

large emitter assembly, (3) possible adsorption of small amounts of oxygen during cooling after the vacuum heating, and (4) slightly different coverages of the constituent elements.

To investigate these factors, a small (1/4-inch diameter) W(100) single crystal was mounted into the SCC. This small sample could easily be heated to 2400 K while maintaining a vacuum of less than 1×10^{-9} torr so that undesirable contamination from outgassing was eliminated. Heating the crystal to 2400 K produced a clean (W - 96%, C - 3%, O - 1%) surface, a sharp (1 x 1) LEED pattern and a work function of 4.66 eV. The literature values for the work function of W(100) are about 4.60 ± 0.10 eV.[3] Thus the heating method is satisfactory and the sample is a well-ordered W(100) single crystal.

Various Zr doses, O_2 exposures at temperature, and vacuum heat cycles were performed with varying initial conditions. The work functions after the vacuum heat treatments remained at about 3.0 eV, instead of the expected 2.7 eV. Slight changes in procedures, and thorough outgassing of the Zr source did not reduce the work function further.

Next, the O and Zr coverages were varied systematically. The crystal was heated to 2400 K for ten seconds, exposed to 10^{-6} torr-sec of oxygen at room temperature, dosed with Zr, and then heated to 1800 K for 10 seconds. This sequence was repeated for several Zr doses. The resulting work function as a function of Zr/W Auger peak heights and O/W Auger peak-to-peak heights is shown in Figure 3. The work function drops steeply to a minimum of 2.74 eV at Zr/W equal to 0.78. This minimum work function agrees with the value of 2.67 $\pm$ 0.5 eV reported in Reference 1. The Zr/O curve is quite similar to the Zr/W curve. Indeed, the O/W ratio only varies from 1.8 to 2.2 while the Zr/W ratio ranges from 0.5 to 2.2.

This nearly constant O/W ratio is twice as large as the O/W ratio in the absence of Zr at 1800 K. Apparently, the Zr strongly binds the O to the W surface at 1800 K.

The next experiments will involve systematically varying the oxygen coverage as well as depositing carbon on the surface to further reduce the work function.

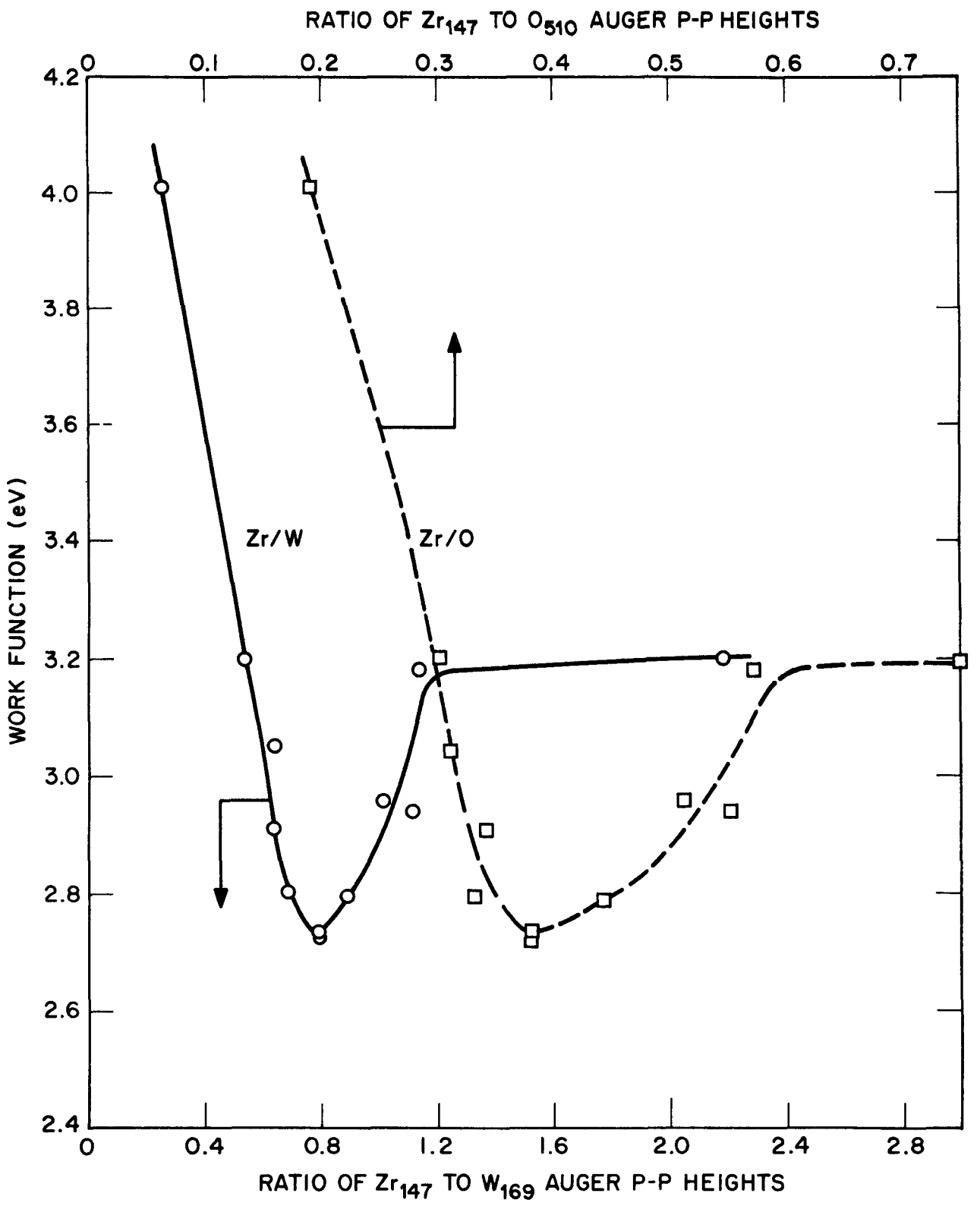

Figure 3. Work Function of Zr-O-W Versus Zr/W and Zr/O for Single Crystal W(100)

A new manipulator assembly has been constructed which allows sample heating and nearly complete viewing of the LEED screen. Also, a new Richardson collector with guard ring is being designed so that emission measurements of work function can be made at high temperatures.

B. Spectroscopic Plasma Analysis

The influence of heavy particle collisions on the excited state distribution of the cesium plasma in a thermionic converter have been studied where the plasma density varies from 10^{12} to 10^{15} cm^{-3} and the electron temperature ranges from 1500 to 3000 K. Since the ionization of a cesium atom is a stepwise process, it is necessary to know the cesium excited state distribution to determine the ionization rates in the plasma. The excited state distribution is also important to determine the electron temperature in the plasma.[4] In studying the cesium thermionic laser,[5] it is essential to know the excited state distribution and the processes involved in order to search for the population inversion conditions.

Many people[6,7] have calculated cesium excited state distributions. In Reference 6, the authors used a set of transition rate equations to calculate the population of cesium excited states in a homogeneous, optically thin plasma. The results predicted that upper level populations approach equilibrium with the continuum, and all levels become closer to equilibrium as the electron density increases. In the case of Reference 7, radiative transitions were not considered and an optically thick plasma was assumed. These calculations indicated that the upper levels are generally not in equilibrium with the continuum. However, in both cases, the theories failed to agree with the experimental results. As shown in Figure 4, both theories predict nearly straight lines, while experimental measurements show a curved distribution.[8,9] Experimental data in Reference 5 also have similiar curved distribution. It is suggested in Reference 9 that atom-atom inelastic collisions should be considered in the calculation to obtain correct results. To estimate the influence of atom-atom inelastic collisions on the cesium excited states distribution, the collision cross sections must be determined. The cross sections for ionization and

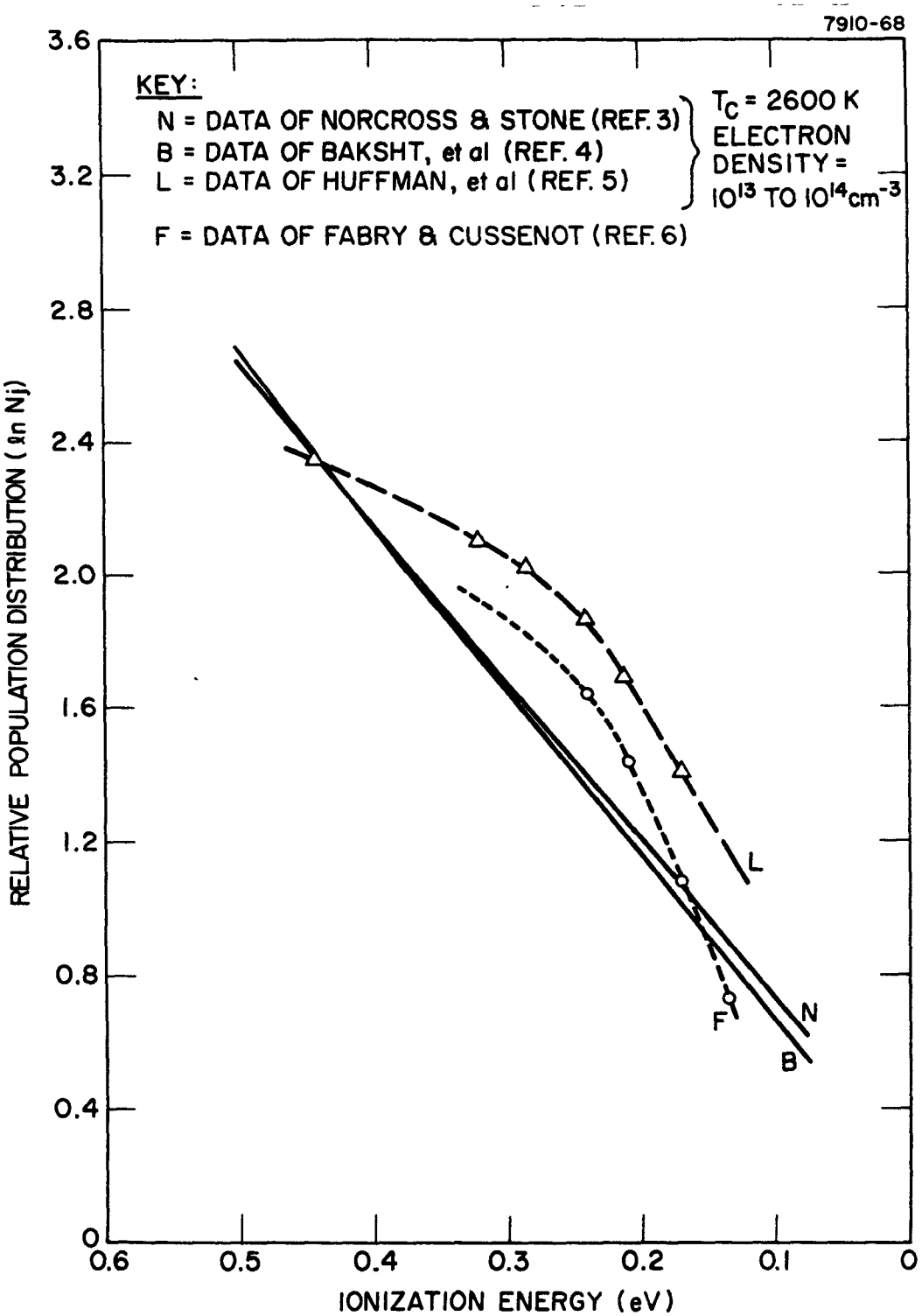

Figure 4. Curve N = Reference 3; Curve B = Reference 4; Curve L = Reference 5. These Three Curves are at T_c = 2600 K, Electron Density at 10^{13} to 10^{14} cm^{-3}, Curve F from Reference 6

excitation of several gases by atomic species have been experimentally determined[10] and theoretically calculated.[11] The cross section of atomic species behave in the conventional manner (i.e, rising with increased impact energy until a maximum is reached, and eventually falling off at sufficiently high energy). The atomic ionization cross section can be estimated using the following model.[12] The amount of kinetic energy available (E_a) for conversion into internal energy between two particles of mass m_1 and m_2 is $E_a[m_2/(m_1 + m_2)]$. If $m_1 = m_2$, the minimum kinetic energy for ionization (E_i) to take place is $2E_i$. The freed electron is carried off with a kinetic energy of $\Delta E_a[m_e/(m_e + m_a)]$ where E_a is the available energy (i.e., $E_a - 2E_i$). In the case of the electron-atom ionization, the freed electron carries off an energy of $\Delta E_e[(m_e/(m_e + m_e)]$ where $\Delta E_e = E_e - E_i$. The Thomson cross section for electron-atom ionization is

$$\sigma_{ea} = \pi e^4 E_e (1/E_i - 1/E_e) = \pi e^4/E_i^2 \left[(V_i - 1)/V_i^2\right] \qquad (1)$$

where $V_i = E_e/E_i$.

We can write

$$\sigma_{aa} = \pi e^4/E_i^2\left[(2m_e(W_i - 2)/(m_a + m_e))/[1 + 2m_e(W_i - 2)/(m_a + m_e)]^2\right] \quad (2)$$

where $W_i = E_a/E_i$, such that the freed electrons have the same kinetic energy in both cases:

$$\Delta E_a\ [m_e/(m_e + m_a)] = \Delta E_e\ [m_e/(m_e + m_e)]$$

The atom-atom excitation and deexcitation cross sections can be estimated in the same manner. Thus, Equation (2) also represents the excitation cross section with $W_i = E_a/\Delta E$ where ΔE is the energy difference of the two states involved in the collision processes.

A comparison between the electron-atom inelastic collision cross section and the cesium atom-atom inelastic collision cross section calculated from the foregoing model is shown in Figure 5. When the energy involved in transition is large, the lower level electron-atom cross section is larger. As the energy in transition becomes smaller, the atom-atom collision cross section becomes larger than the electron-atom's. In the typical cesium plasma of an ignited mode converter, the average kinetic energy of electrons is about 0.20 - 0.26 eV and the average kinetic energy of cesium atoms is between 0.13 and 0.17 eV. For this case, the

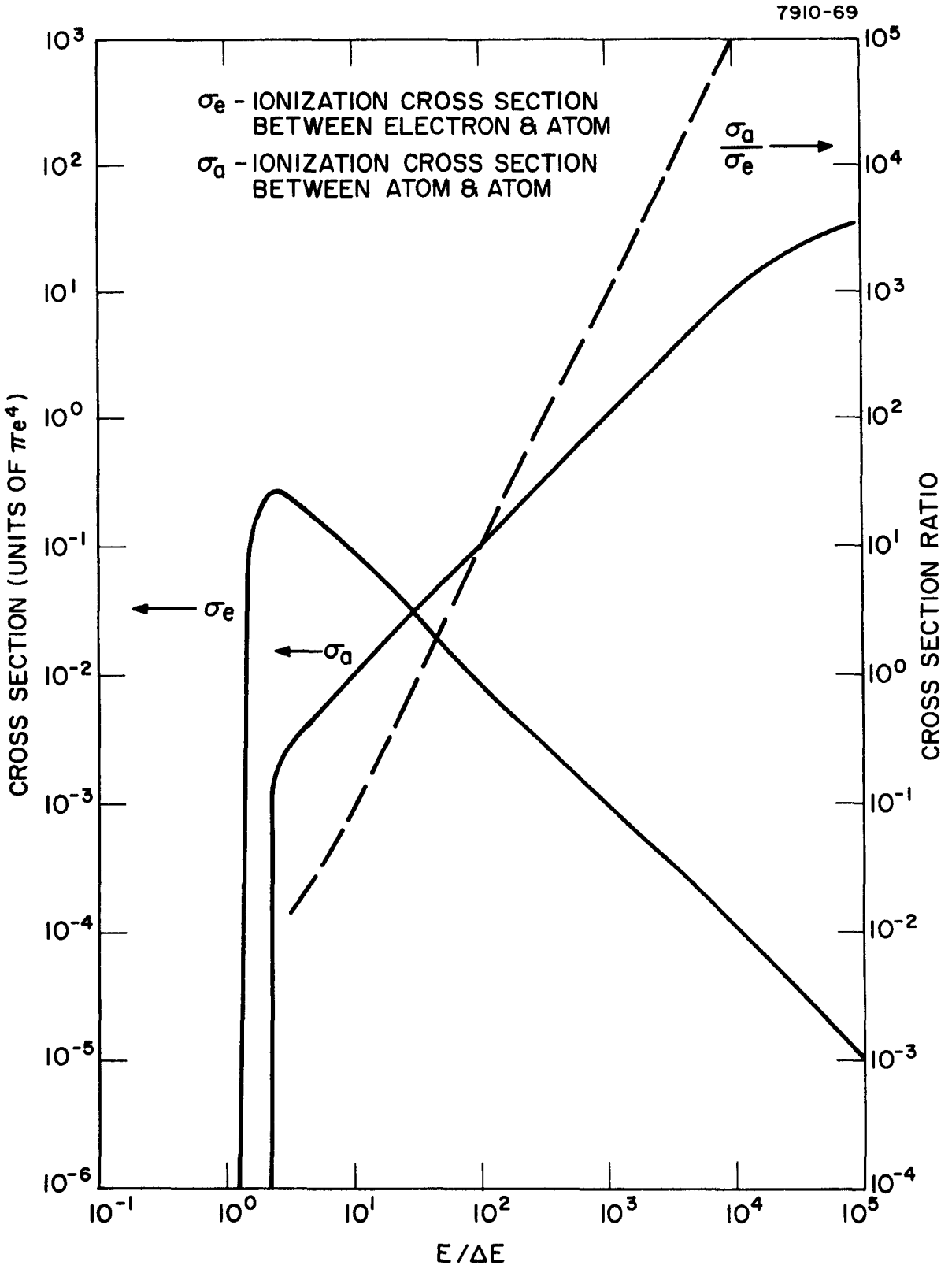

Figure 5. Thomson Cross Section for Atom-Atom Inelastic Collisions. ΔE is the Transition Energy

ionization ratio is about 0.1 - 1%. The low levels of cesium have energy gaps between neighboring states of 0.1 eV and above so that the atom-atom collision effect is small. For the higher excited states of cesium, which are important in spectroscopic measurements and laser studies, the energy difference of the neighboring states are of the order of 10^{-2} eV so that atom-atom inelastic collisions become important. In this case, the distribution of the states will reflect the influence of the atomic species gas temperature rather than the electron temperature which will be measured at these higher states.

By incorporating the atom-atom collisions into the collisional-radiative model to calculate the hydrogen-like gas excited states distribution in the plasma,[13] we obtain the results shown in Figure 6. As expected, the distribution function begins to swing away from the straight line when the energy gap between states is less than 5×10^{-3} eV. Calculations using more rigid cesium coefficients also give similar results.

Since the transition rate is proportional to the particle density and particle temperature, the gas pressure and the gas temperature will affect the excited

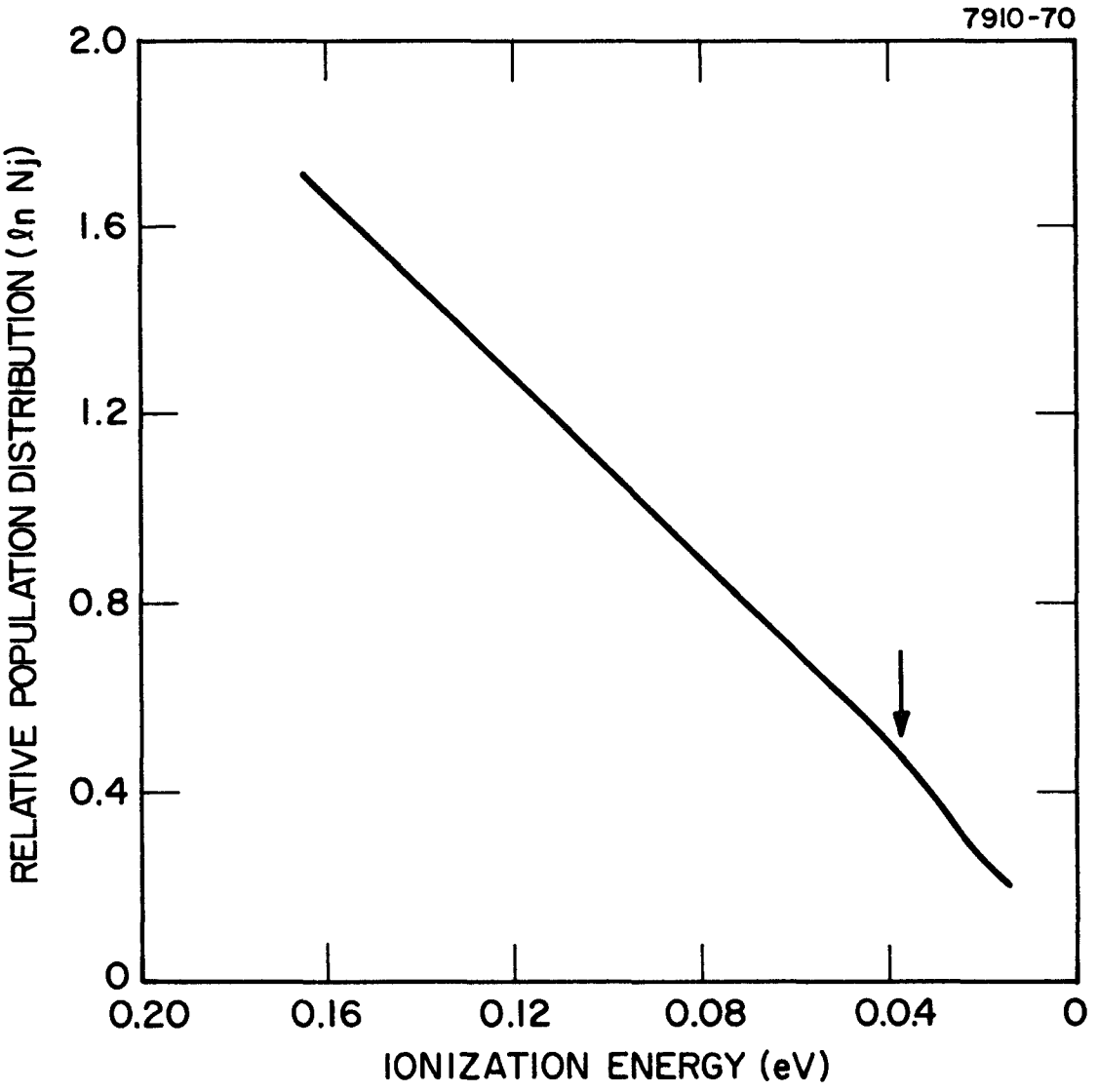

Figure 6. Population Distribution of Hydrogen-Like Gas. Plasma Ionization Potential is 4 eV, T_E = 2600 K, T_a = 1700 K. Distribution Line Curved Over Near the Arrow

state distribution. Therefore, it should be possible to use relative line intensity measurements to determine the gas temperature in the plasma. In addition, it should be possible to achieve population inversions among excited states by adjusting the gas pressure and temperature.

C. Converter Theory

The conditions for the formation of a double sheath between the electrode and the plasma have been evaluated in this reporting period. This module predicts the situations when a double sheath will appear. The results of this study indicate that:

(1) The double sheath will be formed when the normalized plasma density is less than 1.7. This constraint rules out the possibility of the formation of a double sheath on the collector side of the plasma.

(2) The double sheath is formed below the knee of I-V characteristic.

The details of the analysis are given in the Appendix.

1.1.2 TASK II. LOW TEMPERATURE CONVERTER DEVELOPMENT

The objective of this task is to develop thermionic diodes with improved performance at low collector temperatures (i.e., 500-900 K). Converter characteristics will be measured as a function of emitter temperature, collector temperature, cesium pressure, interelectrode spacing and, if applicable, additive gas pressure.

A. Converter No. 207: Tungsten Emitter, Tungsten Oxide Collector

Converter No. 207 was disassembled during this reporting period. Visual inspection revealed a clean reflective emitter and a uniformly grey collector. Although the collector surface showed no signs of peeling, the collector body had cracked into three pieces. The collector will undergo Auger analysis during the next reporting period.

B. Converter No. 215: Heat Flux Diode: Tungsten Emitter, Nickel Collector

Since the last quarterly report, additional retarding plot and heat flux measurements have been made.

Recent retarding plot measurements result in a slightly higher value for the minimum collector work function than previously reported, 1.77 versus 1.70 eV. Collector work function values versus T_C/T_R for the three determinations are given in Figure 7. Output characteristics also indicated an apparent increase in collector work function. The barrier index at T_E = 1400 K is 2.20 eV as compared to 2.12 eV measured previously.

Heat flux measurements at collector temperatures of 850, 750, and 675 K were repeated. These additional heat flux measurements suggest that the value of 2.45 eV reported previously for the collector heating rate at T_C = 750 K may be high. An average of three recent measurements at this collector temperature gave a value of 2.38 eV. Heat flux measurements were also made at a collector temperature of 700 K. Heat production at the collector was 2.40 eV per electron at this temperature. This recent work is summarized in Table II.

A plot of the collector heating rate versus collector work function is given in Figure 8. The slope of the straight line was determined by a least-squares fit.

Measurements will continue on this diode.

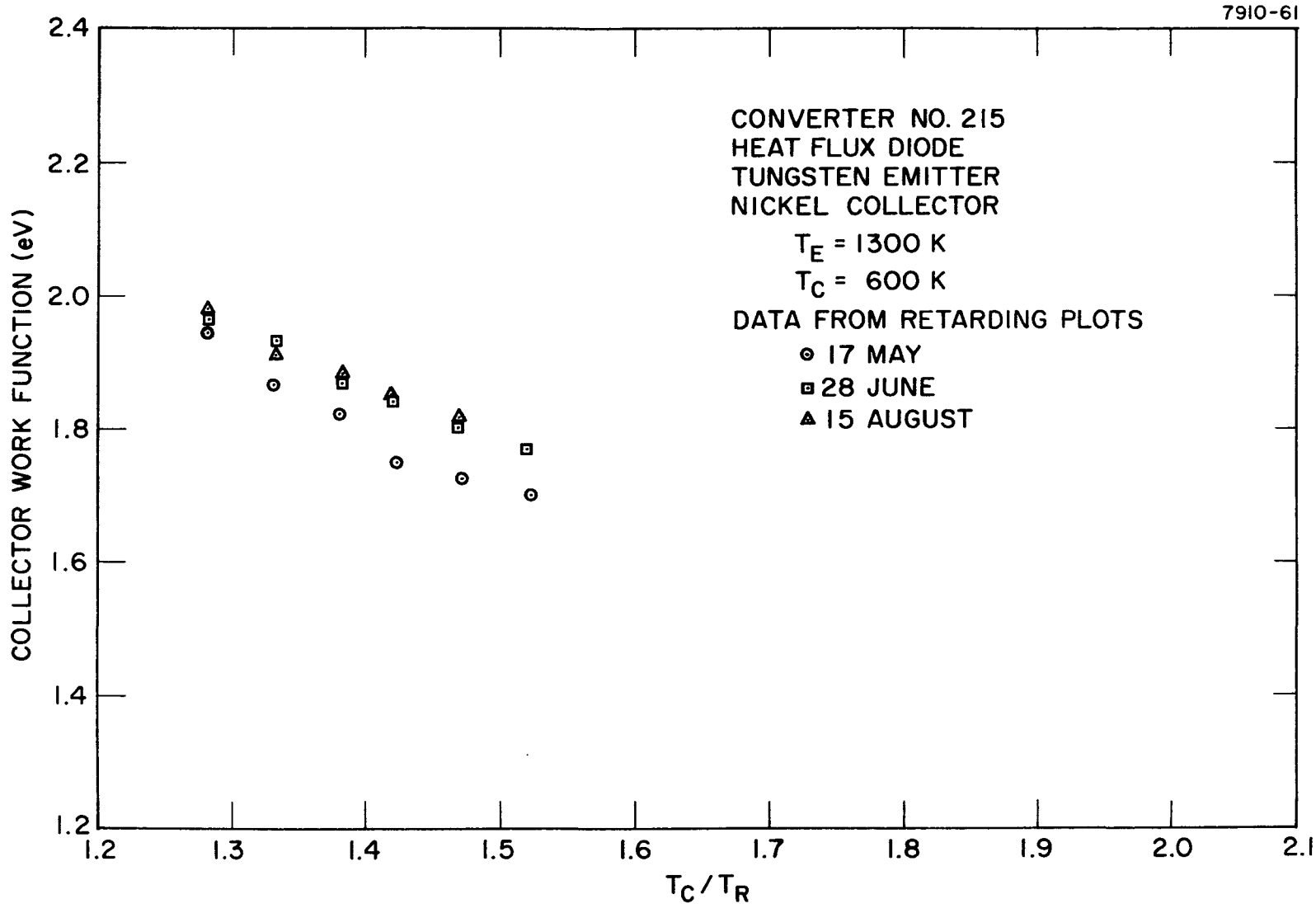

Figure 7. Collector Work Function Versus the Ratio of Collector Temperature to Cesium Reservoir Temperature for Converter No. 215

TABLE II

RECENT COLLECTOR HEAT FLUX DATA

T_E = 1400 K
T_R = 528 K
d = 0.50 mm

T_C (K)	T_C/T_R	ϕ_C* (eV)	Q** (eV)
850	1.61	1.74***	2.27
750	1.42	1.81	2.38
700	1.33	1.91	2.40
675	1.28	1.96	2.47

* Average of Three Retarding Plot Measurements.
** Average Value for Collector Heating Rate.
***Extrapolated from ϕ_C Versus T_C/T_R Plot.

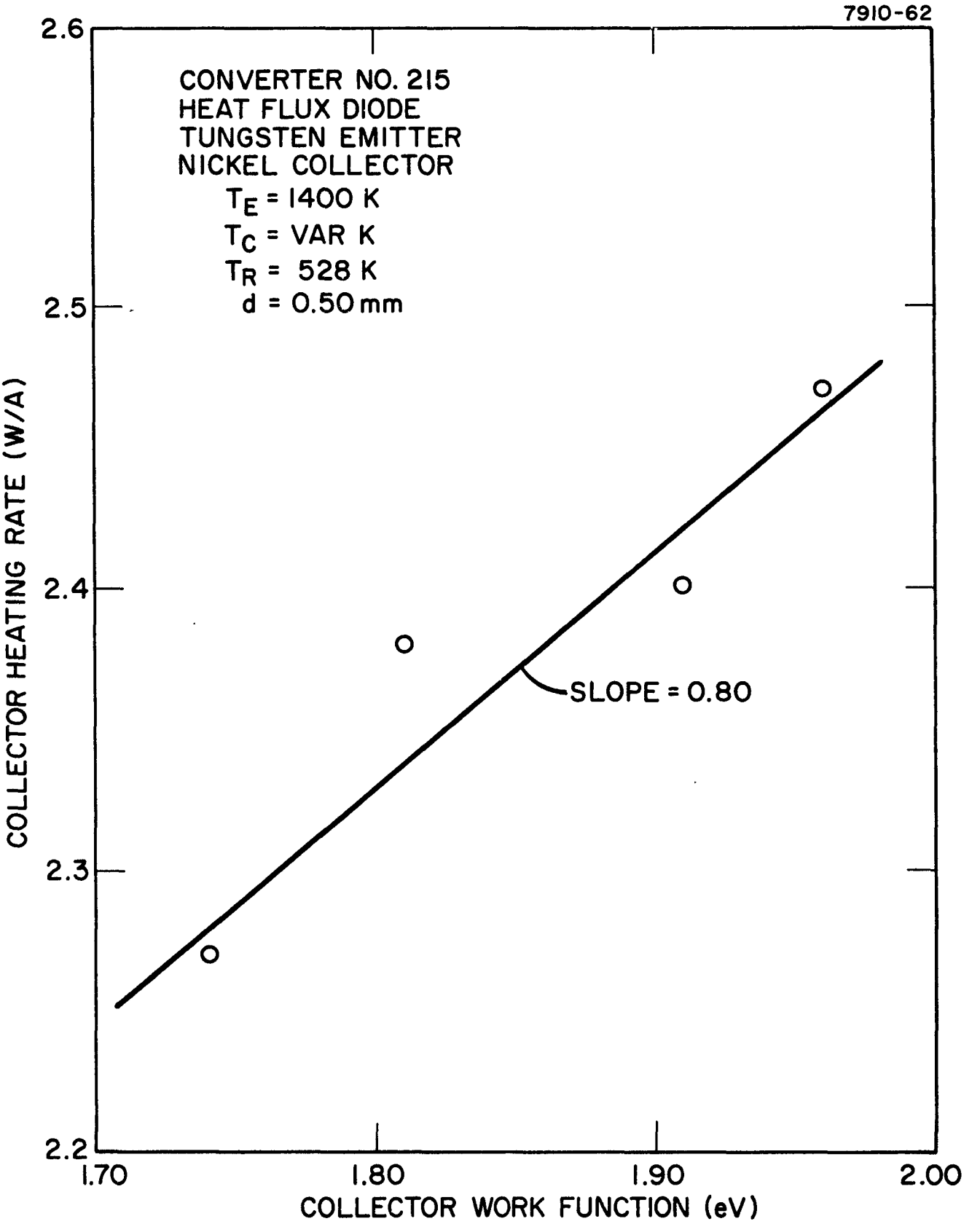

Figure 8. Heat Production at the Collector Versus Collector Work Function

1.1.3 TASK III. ENHANCED MODE CONVERTER EXPERIMENTS

The objective of this task is to formulate and evaluate thermionic converter configurations which have the potential of operating more efficienctly than the conventional ignited mode diode. In the ignited mode, the mechanism for supplying the ions for space charge neutralization is not efficient. Other techniques which allow the converter to operate in the unignited mode (e.g., those utilizing auxiliary discharge regions and surface contact ionization electrodes) should be more efficient in producing ions and, hence, more efficient in converting heat into electricity. Close-spaced devices which do not require ions should also be more efficient than ignited mode diodes. In the ignited mode, structured electrodes offer the possibility of significantly reducing the plasma losses. Several types of enhanced mode converters will be investigated experimentally.

A. Pulsed Triode

A review of previous Thermo Electron data [14] has led to the conclusion that the triode performance was limited by the electron emission from the dispenser

cathode. No further experiments in this area are planned until an emitter with higher current density capabilities is available. Hopefully, the Zr-O-W electrode described in section 1.1.1 will prove suitable for this application.

B. Particulate Ionizer Surface Ionization Triode (PISIT)

This enhanced mode converter concept operates in the unignited mode. The PISIT approach has not been pursued due to the difficulty in fabricating the emitter with a microstructured ionizer surface. However, the microfabrication capabilities of SRI International should enable this organization to build the required emitter-ionizer electrode. This possibility is being explored with Dr. Ivor Brodie of SRI International.

1.1.4 TASK IV. COMPONENT HARDWARE DEVELOPMENT

The objective of this task is to develop converter hardware suitable for operation in a combustion atmosphere such as would be encountered in a thermionic-topped fossil fuel powerplant. Although the effort includes considerable materials evaluation, the focus is on the fabrication and testing of hot shell-emitter subassemblies utilizing chemical vapor deposition (CVD) of composite silicon carbide/graphite/tungsten structures.

A. Alloy Hot Shell Development

The testing of alloy hot shells in the Simulated Furnace continued during this reporting period. In this furnace, the domes of the hot shells are exposed to products of combustion of a liquid hydrocarbon at 1475 K. The interiors of the shells are evacuated by an ion pump. The furnace temperature and the interior vacuum of each shell are recorded on a strip chart recorder. An additional test shell fabricated of RA333 was placed on test on 31 August 1979. The typical composition of RA333 is: Fe 18%, Cr 25%, Ni 45%, Mo 3%, Co 3%, W 3%,

TABLE III

SIMULATED FURNACE TESTS
(16 October 1979)

Test Port No.	Hot Shell	Test Hours	Comments	Date of Initiation
1	446 CRES Cr-Ni Slurry Sinter	2275	Leaktight	20 Nov 1978
3	446 CRES Plasma Arc Sprayed with Cr_2O_3	7749	Leaktight	31 Oct 1977
4	RA333	643	Leaktight	31 Aug 1979
5	446 CRES Plasma Arc Sprayed with Nichrome	7749	Leaktight	31 Oct 1977
6	INCONEL 671	1970	Leaktight	8 Mar 1979

Clock Reference 24753

C 0.05%, Mn 1.5%, Si 1.25%, P 0.015%, and S 0.015%. The accumulated test hours on the specimens are shown in Table III.

B. CVD Hot Shell-Emitter Development

During this reporting period the following accomplishments were achieved.

(1) The CVD process was scaled up to include two hot shells two inches in diameter (two leaktight composite shells were fabricated).

(2) Leaktight SiC was deposited on a graphite shell one inch in diameter 10 inches in length.

(3) Furnace, plumbing, reactants and scrubbing towers for both W and SiC CVD operations were now enclosed in hoods for improved safety.

The following changes were made to scale up the tungsten deposition for the half-scale diode. The WF_6 injector was redesigned to provide extended leaktight operation and better temperature control of the WF_6 gas. The gas flow was increased from 150 ccm to 250 ccm, and the H_2 to WF_6 ratio was optimized. In addition, the injector to shell spacing was refined. The revised apparatus for tungsten CVD is shown in Figure 9.

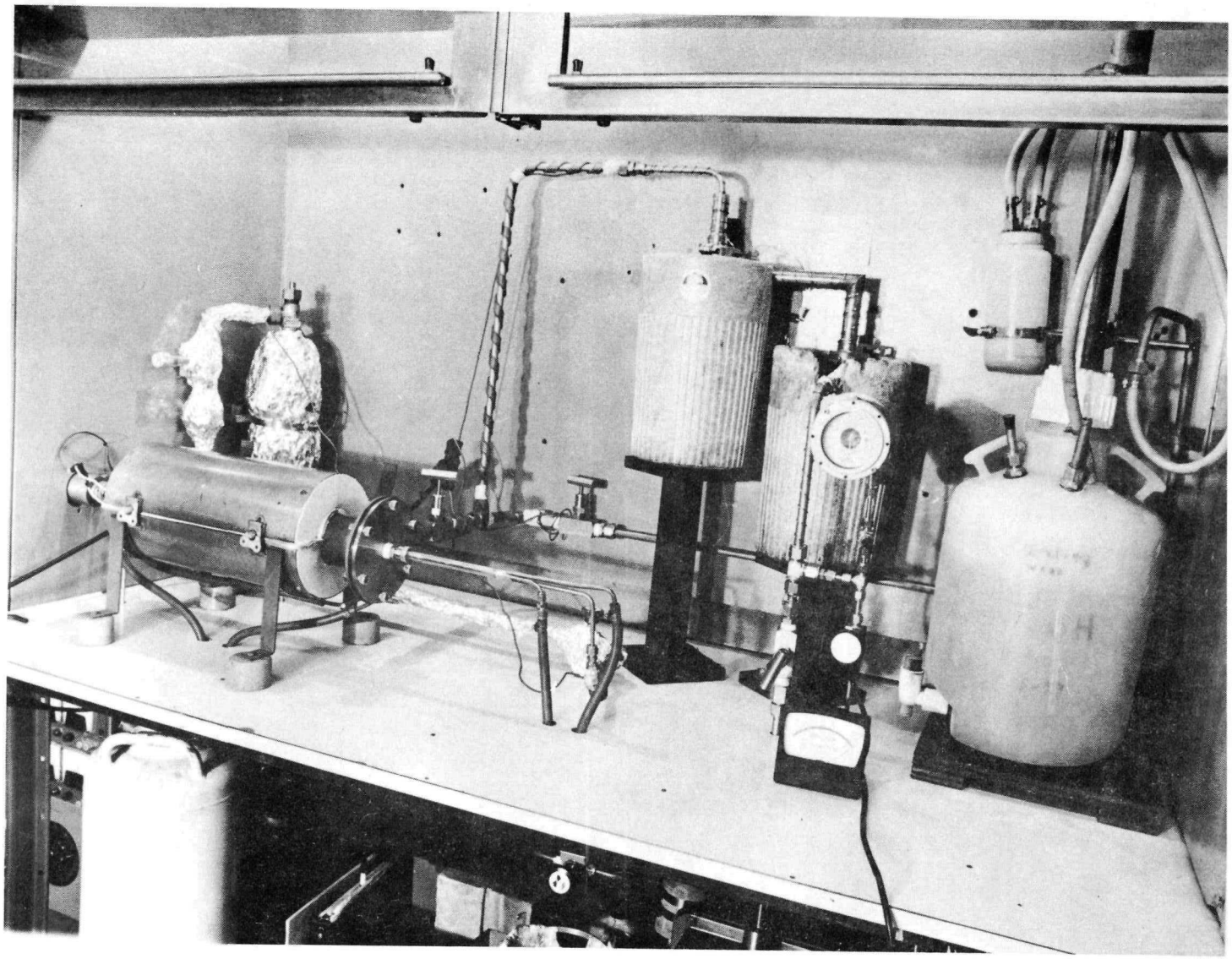

Figure 9 Resistance Heated Furnace for Chemical Vapor Deposition of Tungsten

The following modifications were made to scale up the SiC deposition for the half-scale diode. The size of the graphite concentrator was increased to give a uniform temperature over the nose of the larger, two-inch diameter hot shell. The length of the graphite shell was reduced from 4 to 3 inches in order to maintain a constant temperature of 1250 C over the entire component. The furnace and end plates were redesigned to handle larger shells. Except for increasing the CVD time from 2 to 3 hours, no refinements to the run parameters were made. The improved equipment is photograped in Figure 10. A close-up view of the furnace showing the radio frequency coupling coil is given in Figure 11.

The combination of these changes to the tungsten and SiC CVD equipment and processes resulted in the production of two leaktight composite hot shells two inches in diameter. An assortment of CVD structures fabricated during this reporting period is shown in Figure 12.

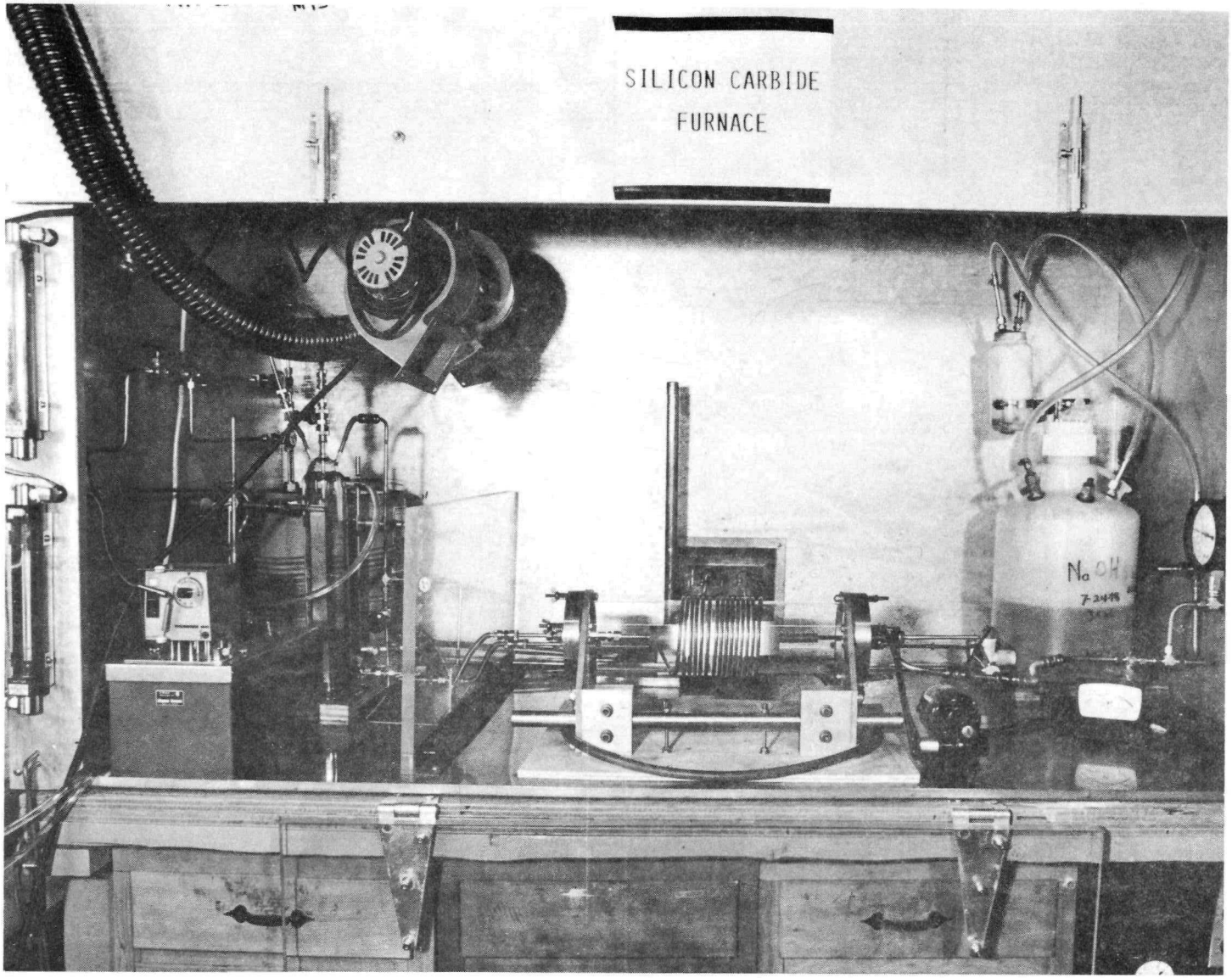

Figure 10 Equipment for Chemical Vapor Deposition of Silicon Carbide

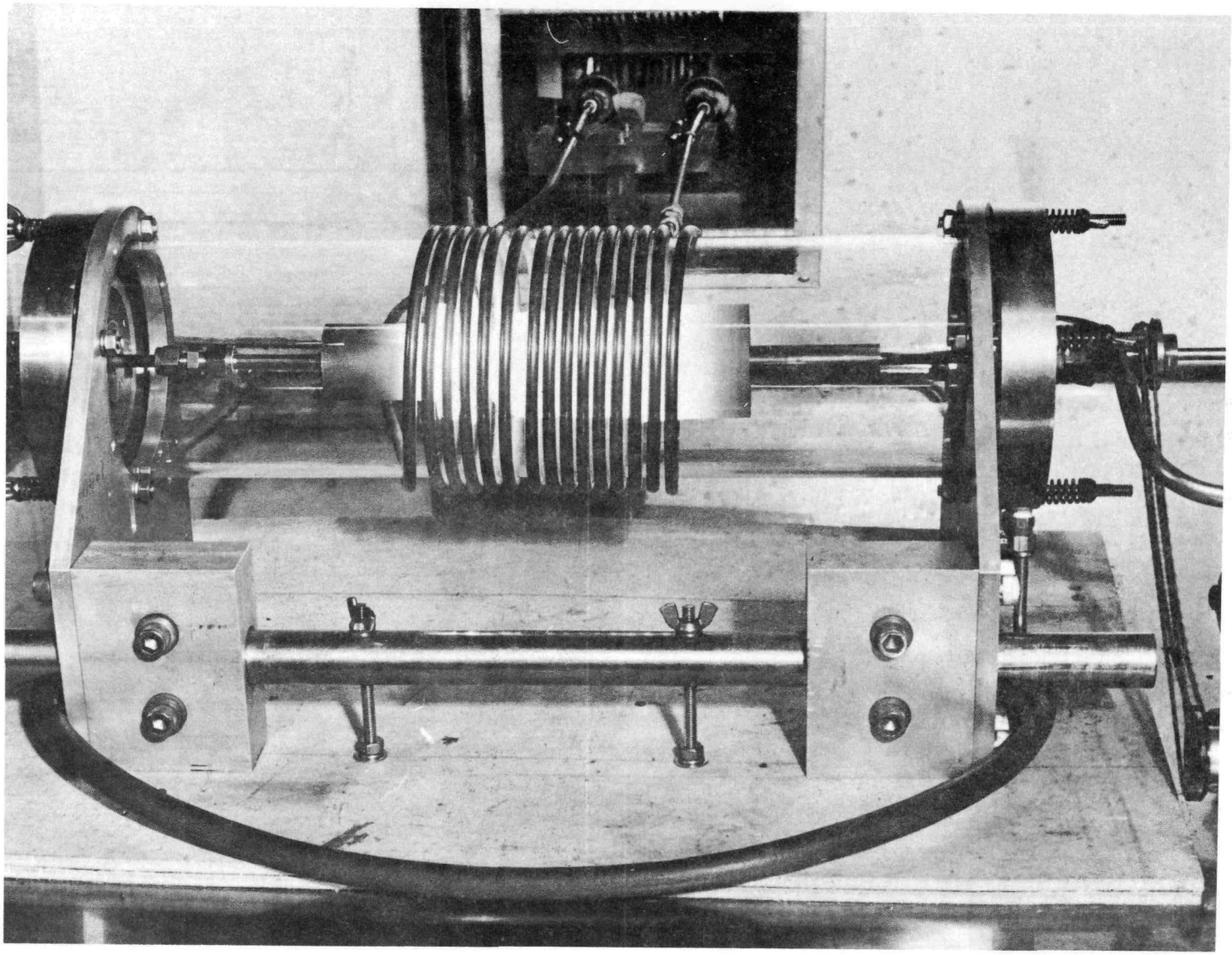

Figure 11 RF Induction Heated Furnace for Chemical Vapor Deposition of Silicon Carbide

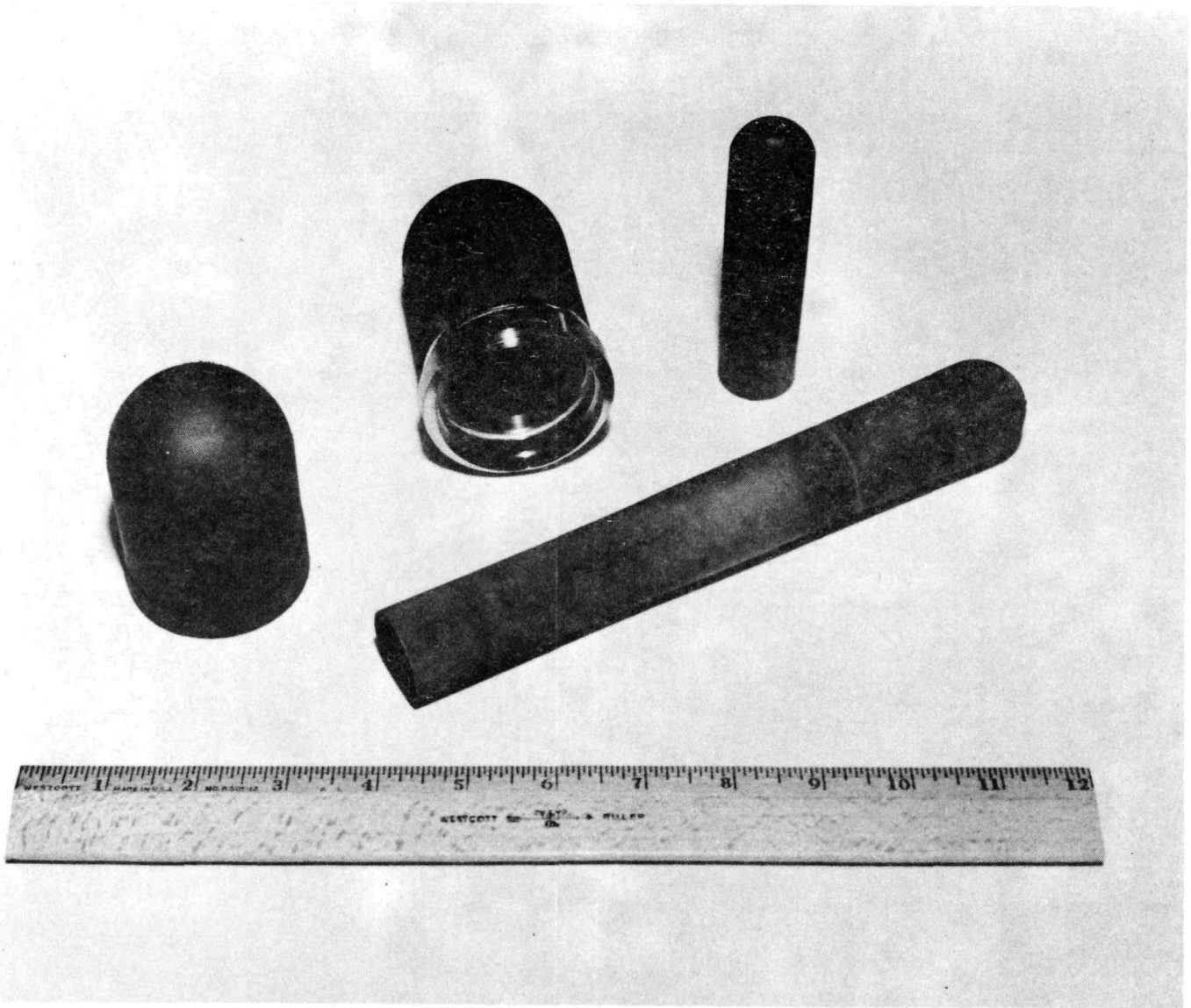

Figure 12 Composite Structures Using Chemical Vapor Deposition of Tungsten and Silicon Carbide

C. Integral Cesium Reservoir Converter No. 222: Tungsten Emitter, Nickel Collector, Cesium-Graphite Reservoir

This converter, which has the same design as Converter No. 208, is being used to study the characteristics of a cesium-graphite reservoir at a higher cesium pressure. The advantage of using a cesium-graphite reservoir is that it can operate at the collector temperature. The converter has two reservoirs; one for liquid cesium, and the other for cesium-graphite (see Figure 13). For a given combination of the reservoir temperatures, the cesium reacts with the graphite to form an intercalation composition in equilibrium with the cesium vapor. After extended operation at a set of cesium-graphite and cesium reservoir temperatures, the cesium reservoir will be removed. The cesium-graphite reservoir then should be able to maintain the cesium pressure for the converter at the soak conditions.

The test conditions for this converter differ from those of Converter No. 208. In this study, the temperature of the cesium-graphite reservoir is 800 K, while that of Converter No. 208 was 750 K. It is desirable to demonstrate that a converter of this type can operate

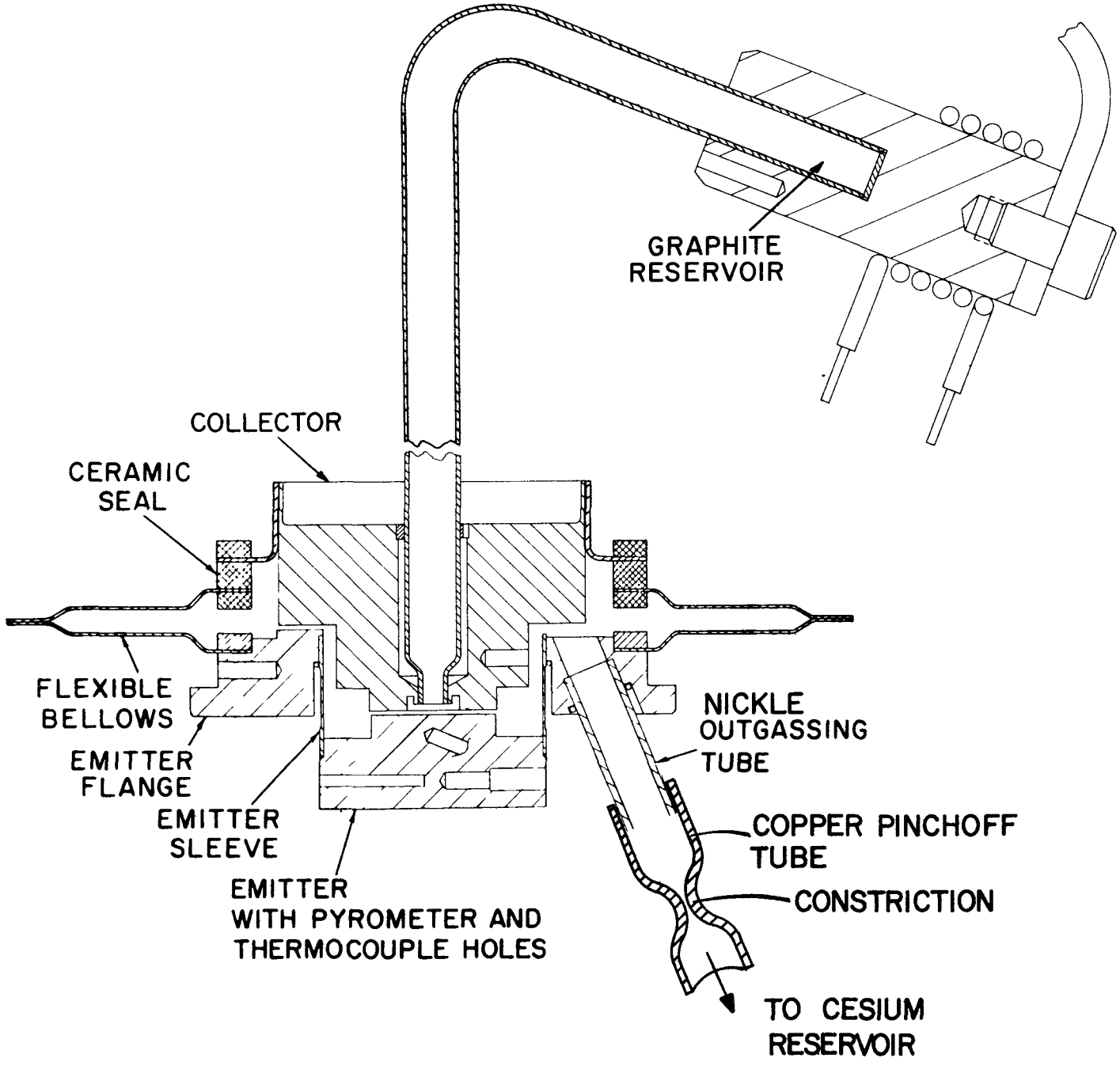

Figure 13. Cross Section of the Graphite-Cesium Reservoir Converter No. 222

over a range of cesium-graphite reservoir temperatures corresponding to varying heat rejection conditions.

Cesium families were taken at an emitter temperature of 1700 K. Figure 14 shows a typical cesium family at a spacing of 0.25 mm and a collector temperature at 750 K.

After these families were taken, the cesium reservoir tube was crimped to slow the pumping action of the liquid cesium reservoir. Testing will continue to determine the effects of the crimp and the subsequent removal of the cesium reservoir.

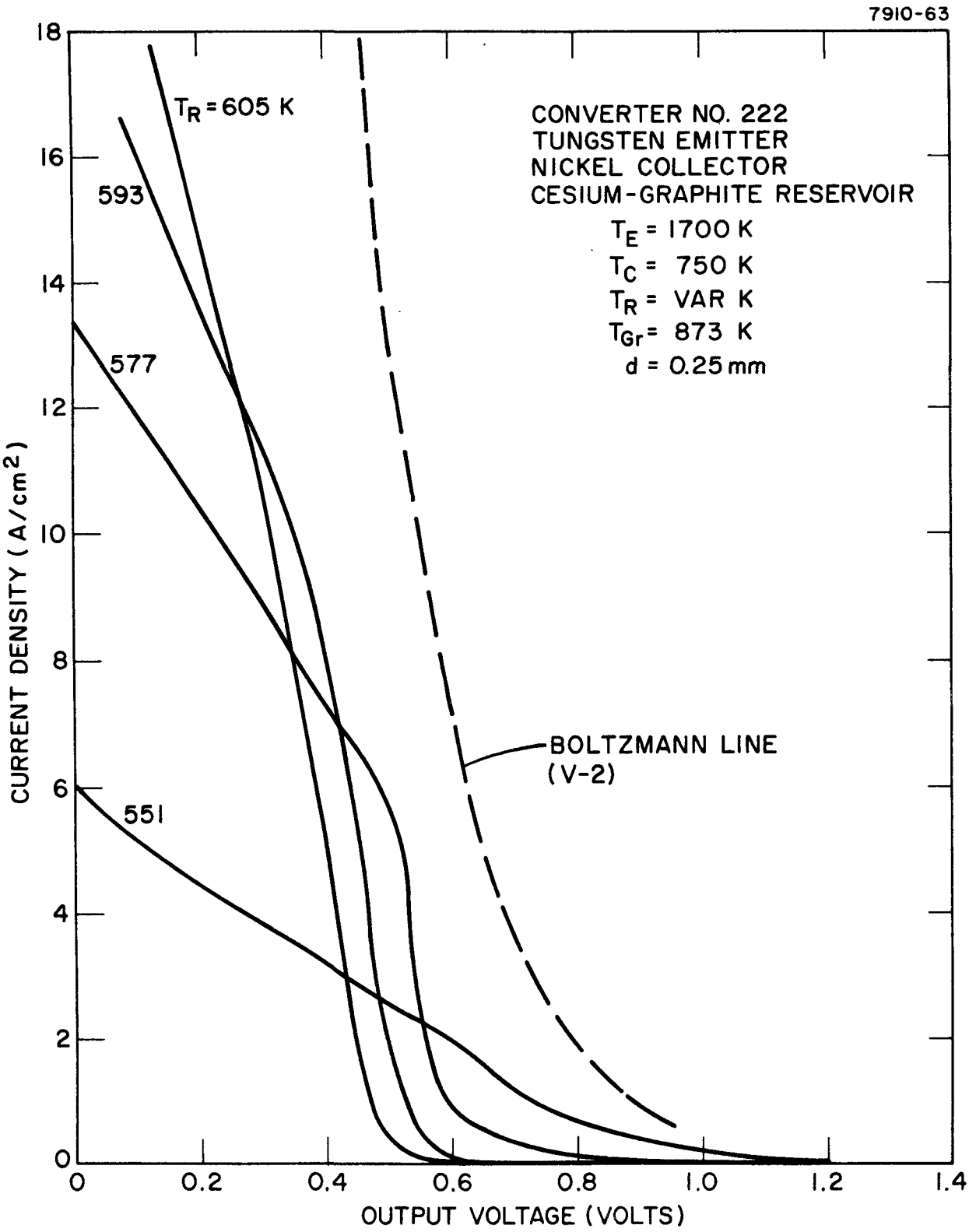

Figure 14. Current Density-Voltage Characteristics as a Function of Cesium

1.2 THERMIONIC POWER MODULE EVALUATION

1.2.1 TASK V. SYSTEM STUDIES

The objective of the system studies task is to identify the design approaches to integrate thermionic energy converters into fossil fuel central station powerplants in the most cost effective manners. The results of these studies will help orient the design of the thermionic array module (TAM) being developed in the next Task VI. Previous system studies carried out in conjunction with Stone and Webster have qualitatively characterized the payoff and penalties of several methods of coupling TAM's into a steam powerplant. The present effort concentrates on quantifying the system options.

Stone and Webster Engineering Corporation has completed their study of a coal-fired thermionic topped central station powerplant. A preliminary draft of this report has been received by Thermo Electron. The approved draft was returned to Stone and Webster for printing and formal submission.

1.2.2 TASK VI. TAM MODULE DEVELOPMENT

The objective of this task is to develop combustion-heated TAM thermionic converters, individually and in small arrays, which are prototypic for topping a central station powerplant. Devices with both alloy and silicon carbide hot shells will be made and tested. In order to define the transient thermal and electrical characteristics of a TAM, a four-diode array will be constructed and tested in the Multi- Converter Test Furnace.

A. Converter No. 218: (CVD Silicon Carbide Converter No. 1): CVD Fluoride Tungsten Emitter Nickel Collector

The life test of this converter continued during this reporting period. The furnace was operated so that the emitter temperature remained constant at 1600 K. As of September 30, this converter has operated for a period of 2315 hours. During this period the converter has been thermal cycled four times to room temperature and twice to 1200 - 1300 K. The performance of the converter has remained stable during this test. At an emitter temperature of 1600 K, the output power density is 2.1 W/cm^2.

A plot of emitter temperature and output power density versus operating time is shown in Figure 15. The life test of this converter is continuing.

B. Converter No. 221 (CVD Silicon Carbide Converter No. 2): Tungsten Emitter, Nickel Collector

The design of CVD Silicon Carbide Converter No. 2 is identical with that of No. 1. This converter was outgassed, cesiated and tested. The performance was quite similar to Converter No. 218 (CVD Silicon Carbide Converter No. 1) except that the optimum collector and cesium reservoir temperatures were slightly lower. The converter had a barrier index of 2.1 to 2.15 eV. The power density at T_E = 1600 K was 2.1 W/cm^2. This power density is identical with that of Converter No. 218. A plot of the power density and emitter temperature versus operating time for Converter No. 221 is given in Figure 16.

After operating at an emitter temperature of 1600 K for 630 hours, the converter developed a leak and was removed from the furnace. The silicon carbide shell was cracked from the hemispherical end to the base, and the graphite and tungsten layers were severely oxidized. The converter was not removed from the furnace quickly

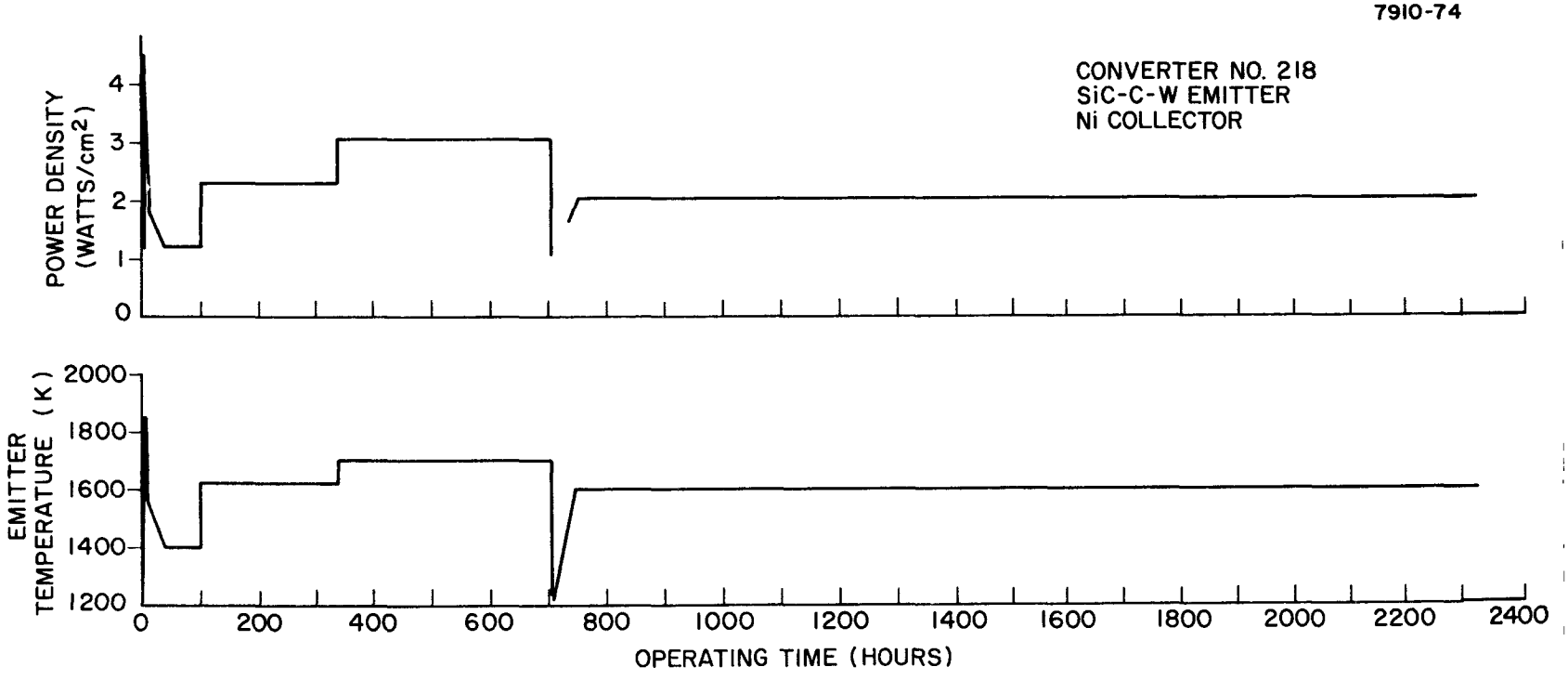

Figure 15. Life Test Profile of CVD Silicon Carbide Converter No. 1

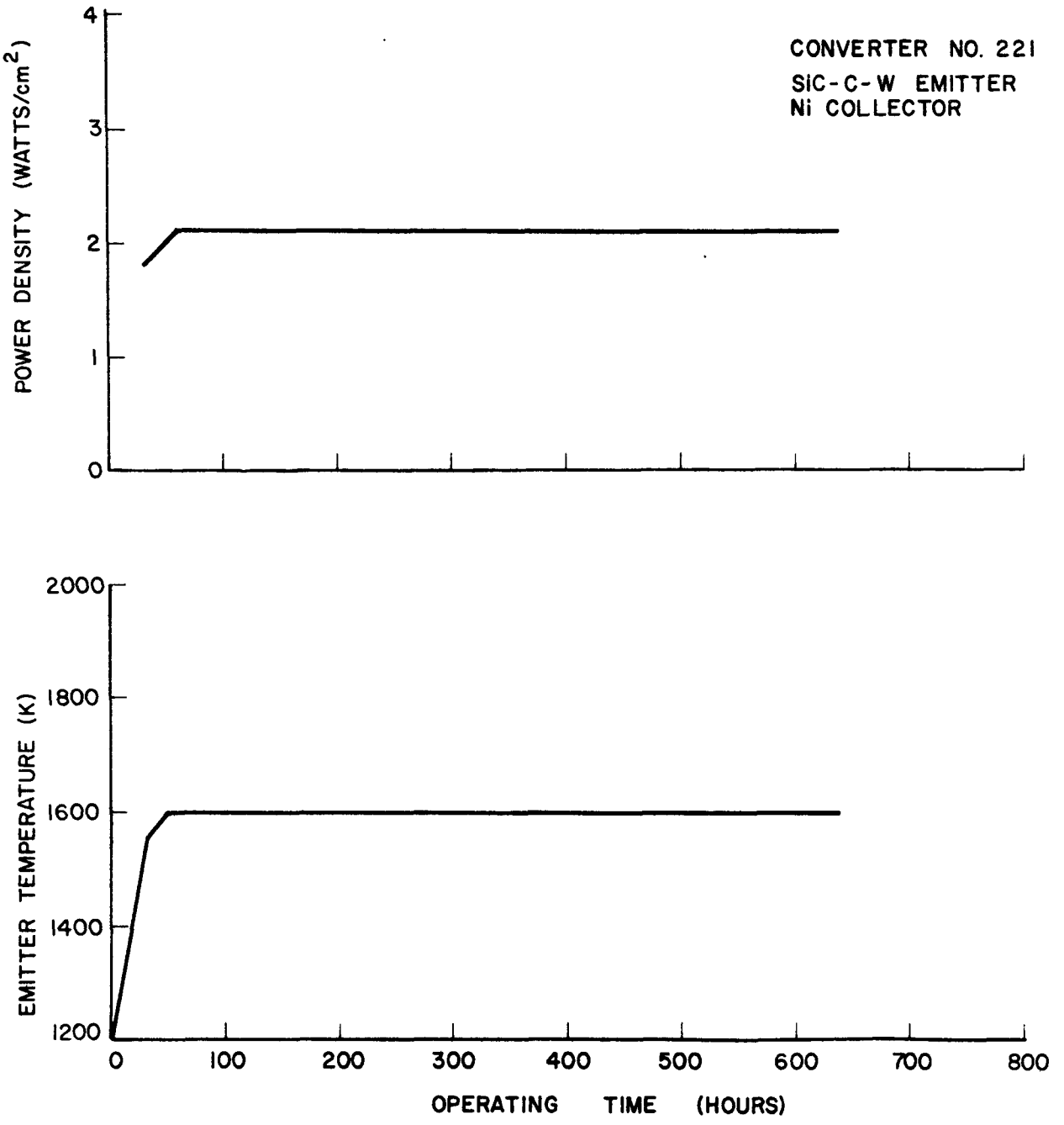

Figure 16. Life Test Profile of CVD Silicon Carbide Converter No. 2

enough to prevent the oxidation that completely masked the original leak. Since this test, techniques for removing converters quickly from the Multi-Converter Furnace have been developed.

C. Converter No. 228 (CVD Silicon Carbide Converter No. 3): Tungsten Emitter, Nickel Collector

The design of CVD silicon carbide No. 3 is the same as Nos. 1 and 2 except for one change. The emitter flange and shell-to-flange braze areas have been protected by nickel plating. It is planned to operate the flange of this converter at a temperature of 850 to 900K.

Converter No. 228 has been assembled and mounted in the Multi-Converter Furnace.

1.2.3 TASK VII. COAL-FIRED TAM TEST UNIT

The objective of this task is to prepare plans for a TAM coal-fired test unit. The preliminary design will be formulated by taking into consideration the results of the system studies and TAM module development. The TAM test unit design will be the smallest size consistent with a realistic simulation of the temperatures, heat fluxes and slag conditions of a coal-fired steam powerplant.

Tentative specifications for the coal-fired TAM test unit have been drafted. Boiler manufacturers are being surveyed for possible test units that might be suitable for TAM evaluation with minimum modification.

2.0 PART TWO: JPL TASKS

2.1 THERMIONIC CONVERTER EVALUATION

2.1.1 TASK VIII. HIGH TEMPERATURE CONVERTER EVALUATION

The objective of this task is to characterize the performance of candidate emitters, collectors and converter configurations at the high collector temperatures (900-1100 K) required for nuclear electric propulsion. Variable spaced, planar converters will be used for this task. Evaluation of each converter will include measurements of the output current density versus load voltage as a function of emitter temperature, collector temperature, interelectrode spacing and cesium pressure.

A. Converter No. 223. (JPL No. 2) Molybdenum Emitter, Tungsten Oxide Collector

A standard variable spaced reseach converter has been fabricated with a molybdenum emitter and tungsten oxide collector. This diode was constructed to study the effects of oxygen dispensation from an oxide collector on a molybdenum emitter. The diode has a sapphire window for visual inspection of the discharge.

Tests have shown that a tungsten oxide collector has a beneficial effect on the molybdenum emitter (see Figure 17). A collector temperature family at T_E = 1400 K, T_R = 507 K and a spacing of 0.50 mm shows a substantial increase in emitter saturation current with increasing collector temperatures.

B. Converter No. 224: Lanthanum Hexaboride Emitter, Guarded Nickel Collector

A mechanically bonded lanthanum hexaboride emitter converter was fabricated and tested during this reporting period. The mechanically bonded emitter utilizes the difference in thermal expansion between LaB_6 and rhenium to reduce the thermal contact resistivity. The design of the emitter is shown in Figure 18. The LaB_6 cap (electric discharge machined from material suppled by CERAC) is fitted snugly onto the rhenium substrate. The higher thermal expansion of rhenium should force a tight fit with the LaB_6 cap to provide electrical and thermal contact. Laboratory tests prior to converter fabrication indicated that a 200-300 degree temperature difference would exist between the LaB_6 and rhenium at emitter temperatures.

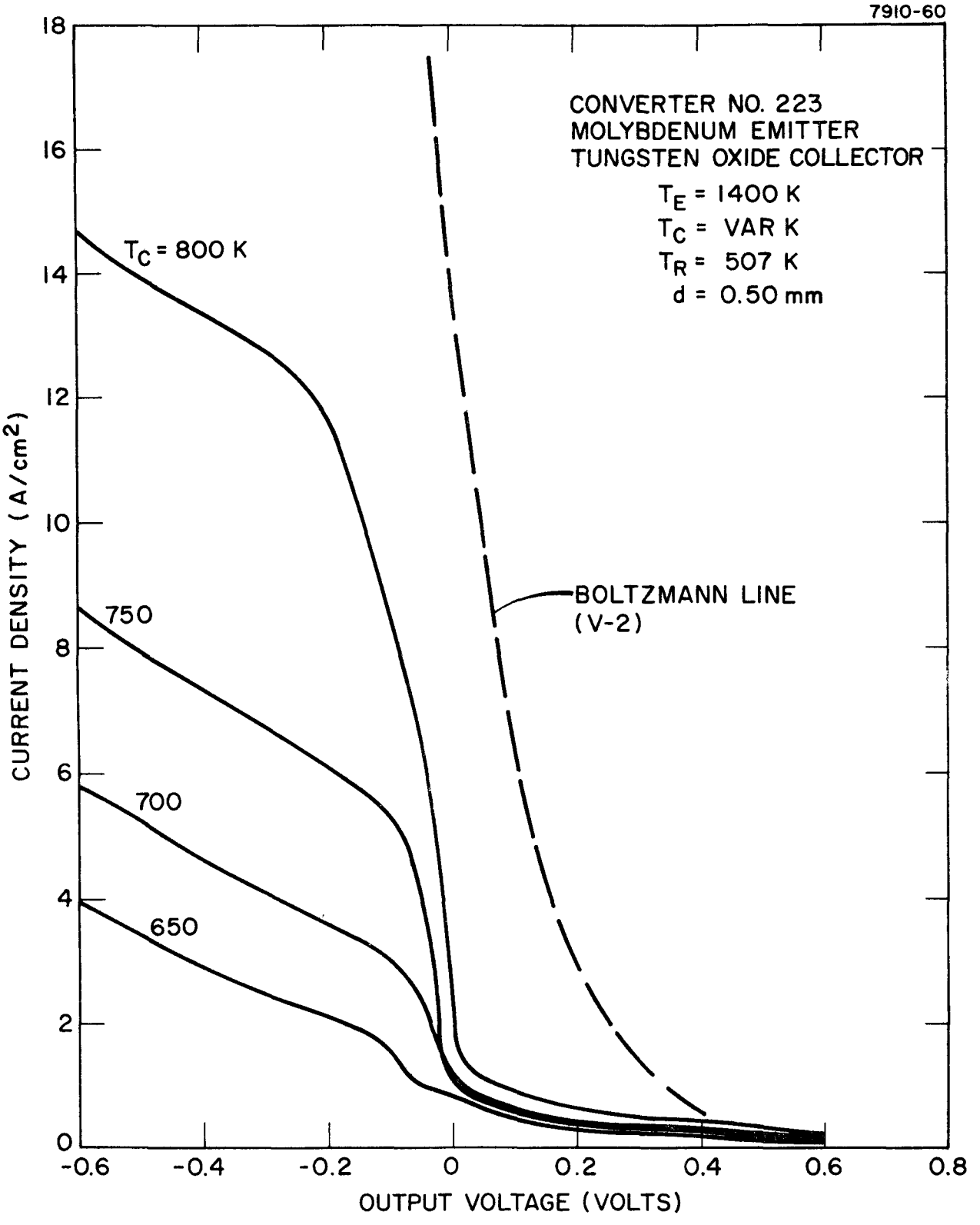

Figure 17. Collector Family for Converter No. 223

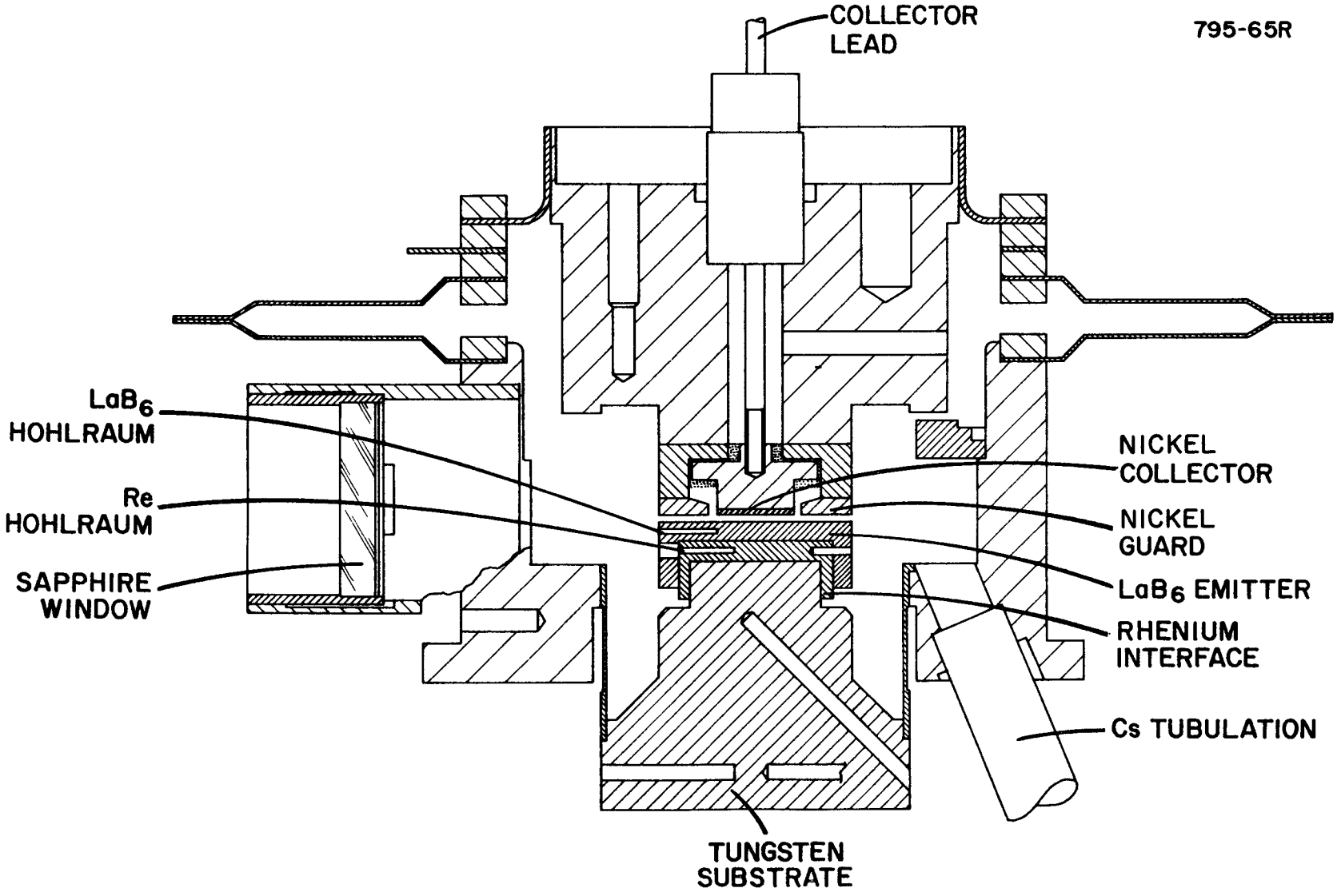

Figure 18. Converter No. 224 with Lanthanum Hexaboride Cap Emitter

In previous converter tests with LaB_6 emitters, it was impossible to distinguish the LaB_6 emission from the emission caused by the portion of the substrate (tantalum) that faces the collector. As a result, no reliable LaB_6 emission characteristics could be measured. This problem is circumvented in Converter No. 224 by: (1) LaB_6 being the only material at emitter temperature facing the collector, and (2) the guarded collector. In addition, the converter is equipped with a window so that the discharge pattern can be monitored.

Prior to cesiation of the converter, a leak was discovered in the emitter sleeve. It was decided to test the converter without cesium since the converter was enclosed in a bell jar that was continuously pumped. Noncesiated LaB_6 emission data were collected. Measurements at 1500 K and 1600 K indicated a LaB_6 work function greater than 4.0 eV.

An attempt was made to clean the LaB_6 surface by heating it above 1700 K. This was accomplished by raising the emitter to the LaB_6-rhenium eutectic temperature (2100 K), for a period of approximately 100 seconds. A bond was formed, as indicated by a swift rise in LaB_6 temperature from 1600 K to 2000 K. After a period of

four hours at 1800 K the emitter was cooled to 1500 K, and emission measurements were taken. The LaB_6 work function was still greater than 4.0 eV.

The LaB_6-rhenium bond did not survive the thermal cycle to room temperature. A second attempt to reach the eutectic temperature failed when the emitter sleeve melted.

C. Converter No. 219 (JPL No. 6): $LaB_{6.5}$ Emitter, $LaB_{6.5}$ Collector

This converter was constructed to evaluate the performance of $LaB_{6.5}$ as both emitter and collector. The material was supplied by LASL as a thin dish for the collector and as a sample bonded to a tantalum emitter substrate. During operation, boron should preferentially evaporate from the emitter (shifting the composition towards $LaB_{6.0}$) and deposit onto the collector surface causing its composition to become more boron rich. Based on LASL data, these conditions were expected to produce favorable electrode work functions.

The emitter substrate was electron beam welded to a Ta sleeve which in turn was brazed to the emitter flange

of the standard variable spacing planar converter. The collector disk was nickel brazed to a molybdenum cap on the standard nickel collector structure. Outgassing was carried out with the pump pressure kept below 10^{-6} torr to minimize oxidation of the electrodes.

After five days of outgassing, an attempt was made to measure the bare work function of the emitter at 1700 K. No current could be measured implying a work function greater than 4 eV. After another four days of outgassing, the emitter was flashed to 1850 K. The pump pressure peaked at 0.1 torr. A work function of 3.66 eV was obtained on cooling to 1675 K. Subsequent measurements after additional outgassing gave an emitter work function of 3.39 eV. In view of the extended operating time at high temperature, it is likely that the emitter had become poorly bonded to the tantalum substrate. Previous experiments have indicated a temperature differential of approximately 150 K between the $LaB_{6.5}$ and substrate for similar structures. Assumption of such a temperature difference implies an emitter work function of 3.03 eV. This value is about 0.5 eV too high to provide practical current densities at 1650 K.

The converter was cesiated by "pinching off" the tube to the pump and distilling the cesium into the reservoir. The converter utilized a reflux reservoir so that it remained connected to an ion pump throughout the testing period. Work function measurements with the reservoir at room temperature gave values of around 3.5 eV, asumming the $LaB_{6.5}$ was at the tantalum substrate temperature of 1675 K. (If the $La_{6.5}$ were 150 K cooler than the substrate, the emitter work function would be 3.2 eV).

Cesium families of J-V curves for the converter were obtained over the emitter temperature range from 1300 K to 1700 K at spacings from 0.13 to 1.0 mm. At the lower temperatures the data show very poor performance with barrier indicies of about 3 eV. The curves appear resistive and may be the result of side discharges to the tantalum substrate rather than from current across the interelectrode gap between the LaB_6 electrodes. This conclusion is further reinforced by the unusually small variation in the characteristics with changes in spacing. A larger temperature difference between $LaB_{6.5}$ and the tantalum would greatly reduce the electron emission from the $LaB_{6.5}$ surface and would result in most of the current coming from the hotter substrate.

The performance gradually improved during operation at an emitter temperature of 1700 K. Another set of cesium family J-V curves were taken after 50 hours of soaking when the performance had stablized. The barrier index was now approximately 2.5 eV at 5 A/cm^2 and continued to show resistive and side discharge characteristics. Perhaps the extended operation at 1700 K improved the bonding.

Collector work function was measured by both retarding potential and back emission techniques. Retarding plots gave a minimum $_C$ of 1.43 eV at a T_C/T_R of 1.18. Back emission measurement gave a $_C$ of 1.22 eV at a T_C/T_R of 1.34. Both values are questionable because of the importance of side emission in the power data. The retarding value is especially suspect because of the uncertainty in emitter temperature.

The converter results discussed cannot be considered definitive of LaB_6 in a converter environment. The configuration of the test converter and the arrangement of the outgassing and cesiation equipment made it unlikely that the electrode surfaces could be cleaned sufficienty to be consistent with high vacuum chamber determinations. Further, the probable poor bonding of the

$LaB_{6.5}$ to the tantalum substrate makes the perfomance measurments unreliable. However, if $LaB_{6.5}$ material had given the high emission expected, the data would have indicated the resultant high currents in spite of the poor bonding. Definitive testing of $LaB_{6.5}$ material in a converter environment will require both better bonding to a substrate and an improved converter design which will maintain extremely high vacuum during the outgassing and cesiation stages.

This converter has been shipped to JPL with the reflux tubulation pinched off.

2.1.2 TASK IX. ADVANCED CONVERTER STUDIES

In the conventional ignited mode diode, transport losses due to ionization, and coulombic and neutral atom scattering greatly reduce conversion efficiency. The objective of this task is to demonstrate improved thermionic converter performance by means of reduced potential loss in the interelectrode space. Based on previous studies, the particle thermionic converter (PTC) has been chosen for further investigations. Specifically, the electrical and thermal properties of PTC configurations will be tested as a function of particle composition and electrode spacing.

A. Particle Thermionic Converter

Experiments were conducted to investigate the temperature profile in a particle thermionic converter (PTC). The temperature drop across the PTC can be broken into two parts: the sum of the temperature drops across the individual particles and the sum of the temperature drops across the particle-to-particle contacts. It was anticipated that the particle-to- particle contacts would constitute a highly resistive thermal path relative to that of the solid particles. This would be reflected in high particle-to-particle temperature differences as compared to those across the solid particles.

N-type silicon-germanium, a semiconductor with a known Seebeck coefficient, was applied as a sprayed coating between two molybdenum electrodes. For a given temperature difference, the open circuit voltage between the two electrodes will be equal to the mean SiGe Seebeck coefficient multiplied by the total temperature drop across the SiGe particles. The temperature drop across the particle interfaces will not contribute to this thermoelectric voltage. A comparison between the measured open circuit voltage and the calculated open circuit voltage that would be generated from solid SiGe for a given temperature difference across the particle matrix will reflect the proportion of the temperature drop associated with the particle interfaces.

The experiment was performed inside a vacuum bell jar. Initially, both electrodes were heated to the same temperature. The emitter temperature was then slowly raised and the open circuit voltage was recorded at various electrode temperature differences ranging from 100 to 500 K. The temperature drop through the solid particles was computed from the open circuit voltage. The results for two collector temperatures are plotted in Figure 19. Based on the foregoing model, over 50 percent of the temperature drop appeared across the solid particles.

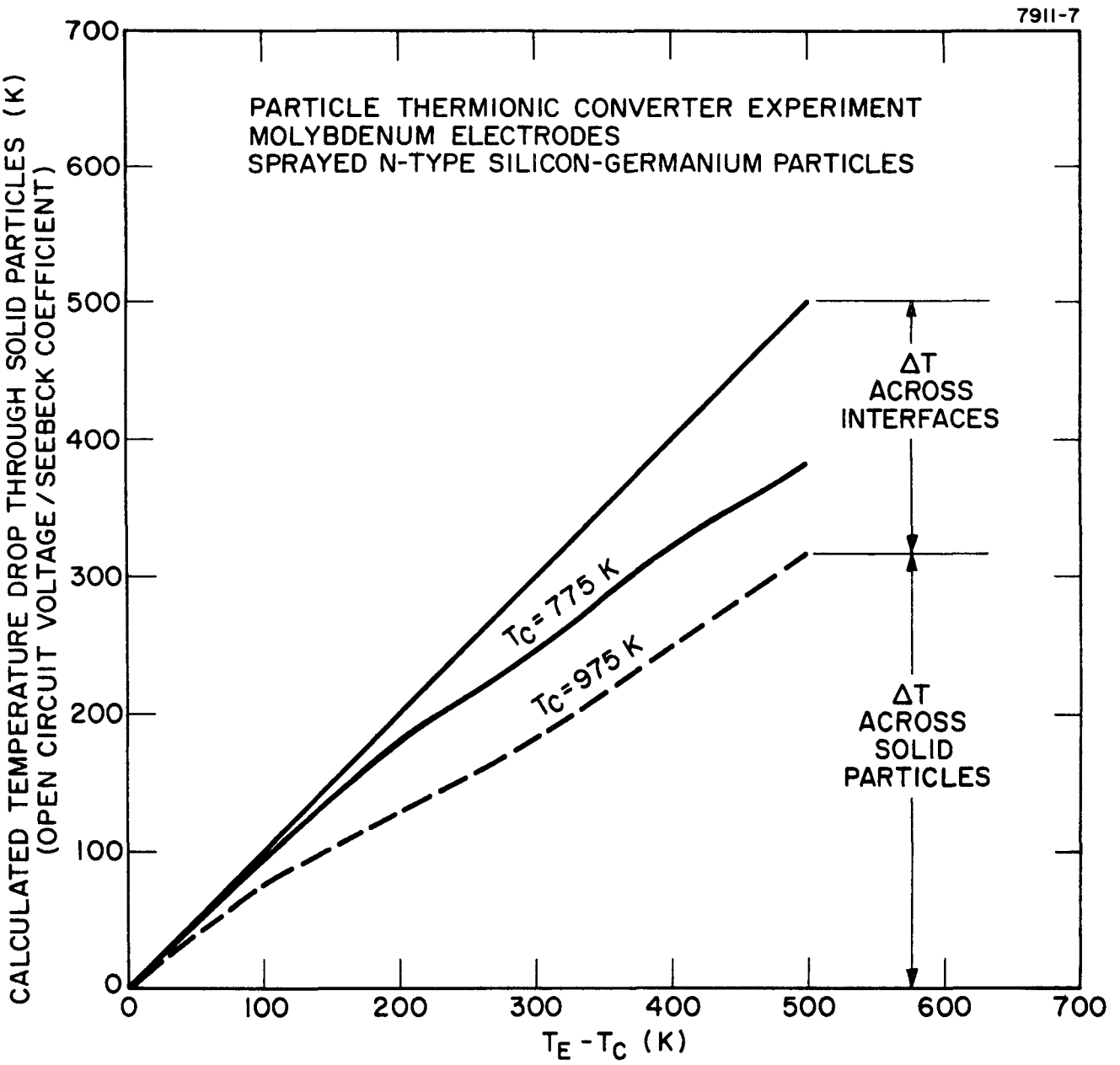

Figure 19. Characteristics of Temperature Drop in Si-Ge Particle Diode

2.1.3 TASK X. POSTOPERATIONAL DIAGNOSTICS

The variable spaced planar converters built for JPL are deliverable items. However, if it appears advisable on mutual agreement between JPL and Thermo Electron, selected converters shall be opened for post operational diagnostics after performance testing. The objective will be to identify the degradation mode, if any, and identify the probable mechanisms of formation.

A. LaB_6-Re Bond Test

A technique for forming a LaB_6-Re bond has been developed and tested. A round wafer of CERAC LaB_6 was placed in a Re cup, and the whole assembly was heated very briefly to 2105 K. At this temperature, a Re-B eutectic was formed which tightly bonded the LaB_6 and the Re.

The cup was transferred to the Surface Characterization Chamber for temperature, FERP and Auger measurements. The LaB_6 was 23 K cooler than the Re cup at 1600 K, indicating good thermal contact. The initial FERP work function of the LaB_6 was 3.9 eV. The FERP work function dropped to 3.4 eV after one minute at 1500 K, to 3.2 eV after 30 minutes at 1700 K, and to 3.0 eV

after five minutes at 1900 K. The thermionic work function was 2.8 eV after a five minute heat treatment at 1900 K. Thus the LaB_6 was activated by high temperature firing in ultrahigh vacuum ($P < 1 \times 10^{-9}$ torr for all measurements).

The LaB_6 surface became slightly contaminated by Mo or Mo oxides desorbing from the hot collector during further high-temperature thermionic measurements. Some cracks developed in the LaB_6 during the heating cycles due to the difference in thermal expansion between Re and LaB_6. These cracks, which were not in a direction to impede heat or current flow, are indicative of good bonding.

After 168 hours of operation from 1600 to 1700 K, the temperature difference between the LaB_6 and Re was less than 30 K. Thus the bond was better than any evaluated previously at Thermo Electron. The high LaB_6 thermionic work function of 3.2 eV and greater during the life test may be related to the Mo contamination. High emission (effective work function of 2.75 eV) were observed from the Re cup and the interface region.

The cup assembly was sent to Photometrics for Auger analysis. The areas analyzed are shown in Figure 20 and the elemental compositions of these areas are shown in Table IV. Analyses of areas moving from the center spot outwards are given in Runs 1-6. The interface regions in Run Nos. 3 and 4 contain the most La and B, but less Mo. This observation is consistent with the large emission from the edge of the sample. The braze-like area (Run No. 5) and the Re cup (Run No. 6) contain a larger amount of Re and essentially no boron. Evidently the Re-B eutectic flowed over the edge of the LaB_6 and then the B diffused into the Re during the prolonged heating. Some lanthanum has also diffused on the Re cup.

A cross-sectional slice through the cup is shown in Figure 21. The purple top center portion of the sample is LaB_6. The thin dark purple band noted on the surface in Figure 20 is not visible in the bulk. The grey area in Figure 20 does extend into the bulk and is probably LaB_4 formed by rapid diffusion of B out of LaB_6. The lighter grey bond region below the LaB_4 is probably the Re-B eutectic which filled the gap when liquid. A thin (0.016 mm) grey area is visible.

TABLE IV

ANALYSIS OF PHOTOMETRICS DATA
LaB_6 - Re Cup

Element	RUN NUMBER												
	1	2	3	4	5	6	7	8	9	10		A	B
La	24	23	28	16	30	9	27	32	31	28		22	22
B	10	10	18	1	20		15	13	31	22		45	20
C	45	37	22	14	20	29	32	28	19	13		6	8
O	18	18	20	18	22	11	21	22	13	19		7	12
N	0.3	0.2	0.2				0.4	0.4	0.3			1	1
Mo	2	12	2		7	1	4	3	4	5		16	
W	1												
Re			10	51	1	49				12			37
Ar							0.6	0.7	0.6	0.4			
S												2	

Table gives percent coverages for Photometrics Runs 1-10. Included also are Runs A and B made in TECO Surface Characterization Chamber - June 21, 1979.

Run No.	Region
1	Center Area - Pink Spot
2	Center Area - Adjacent to Pink Spot
3	Dark Purple Band - Near Interface Between La_6 and Re
4	Grey Area - Interface Between LaB_6 and Re
5	Braze Like Area - Interface Between LaB_6 and Re
6	Re Substrate
7	Center Spot - 10 Sec. Sputter
8	Center Spot - 30 Sec. Sputter
9	Center Spot - 2 Min. Sputter
10	Grey Area After Sputter
A	Near Center Area. Compare to Run No. 2
B	Silvery Deposit on Re Cup

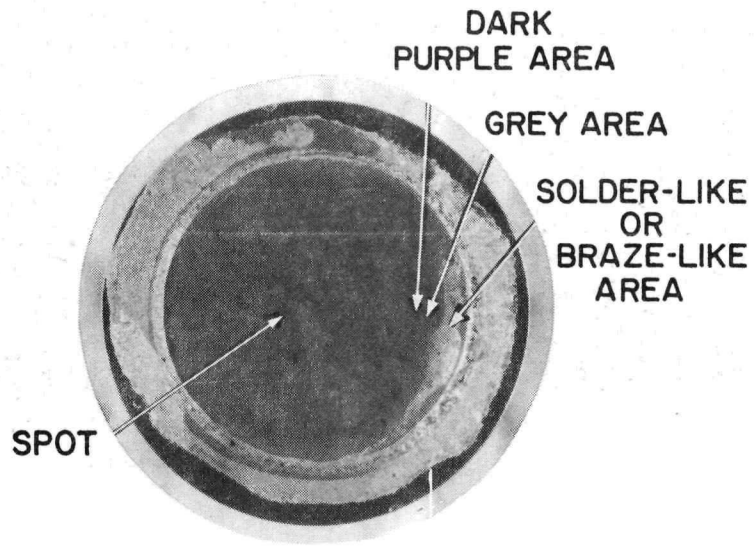

Figure 20 **Photograph of Lanthanum Hexaboride Bonded to Rhenium Cup**

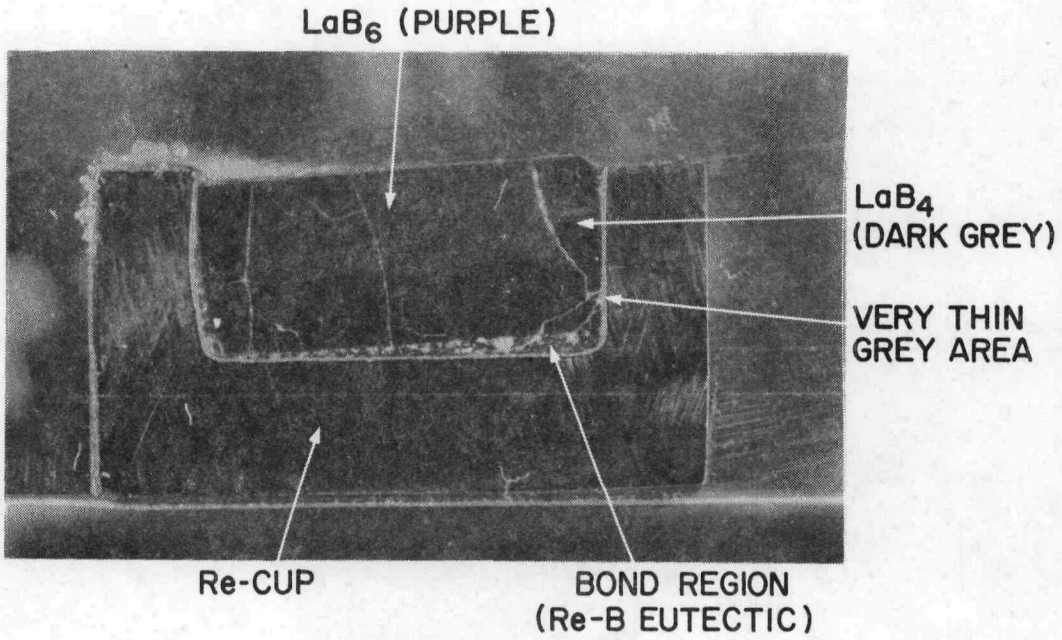

Figure 21 Cross Section of Lanthanum Hexaboride Bonded to Rhenium

Thus, this eutectic formation technique gives a good LaB_6-Re bond which is stable at 1600 to 1700 K for more than 150 hours.

2.2 CYLINDRICAL CONVERTER DEVELOPEMTN

2.2.1 TASK XI. CYLINDRICAL CONVERTER COMPONENT DEVELOPMENT

The objective of this task is to develop the technology required to construct cylindrical converters, excluding the electrode surfaces. This task includes electrode insulation, seal-bellows subassembly and thermoelectric lead components.

A. Electrode Insulation

The out-of-core thermionic reactor design for nuclear electric propulsion requires electric insulation at the emitter temperature (1650 K) with only a small temperature drop across the insulation. Sapphire is a candidate material for this application.

A technique for casting sapphire between molybdenum cylinders with diameters prototypic of the present NEP thermionic reactor system design has been developed. The assembly for casting is shown in Figure 22. The sapphire reservoir is charged with crushed Lucalox, and the assembly is heated by RF in a hydrogen atmosphere.

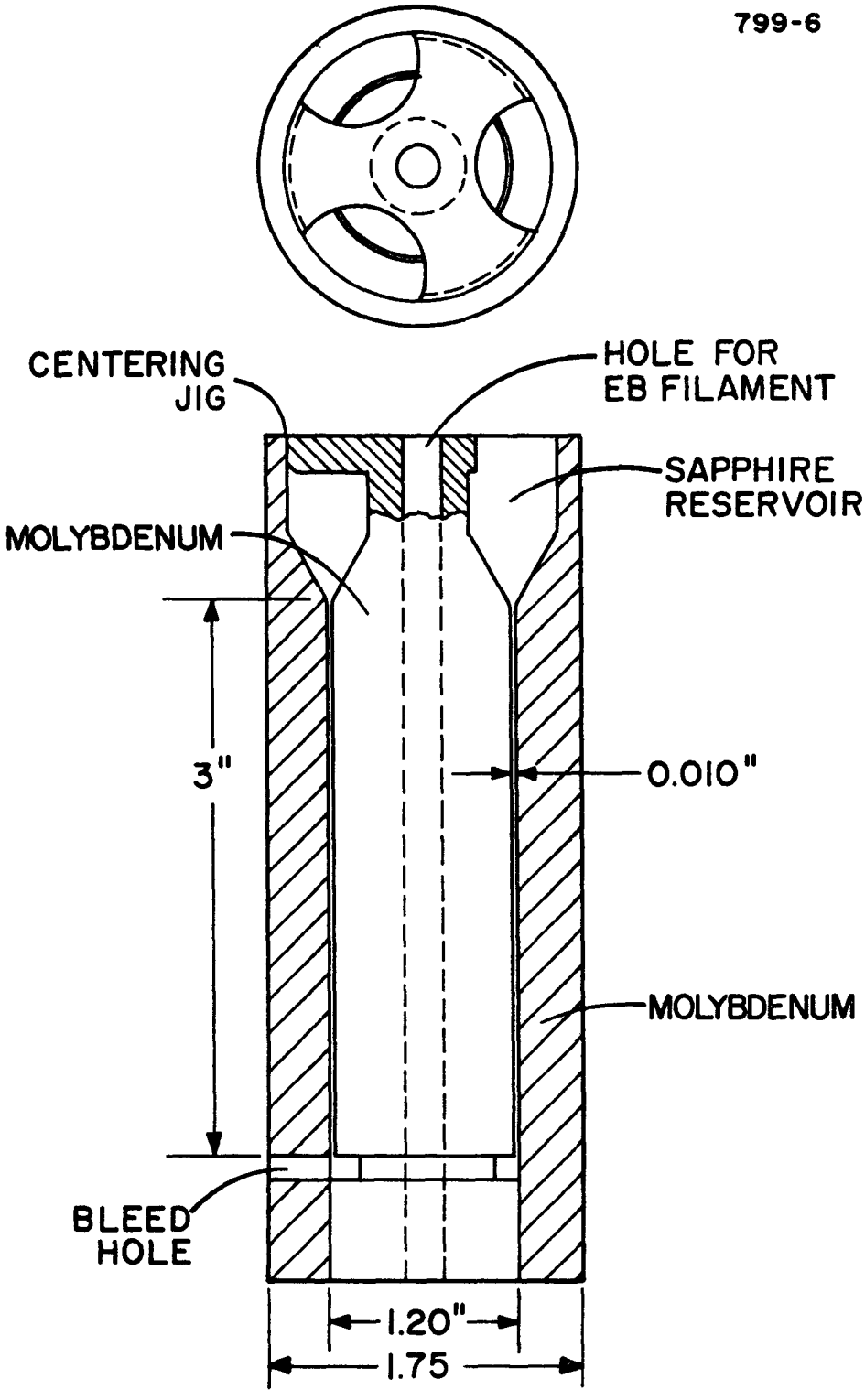

Figure 22. Assembly for Casting Sapphire

The molten sapphire fills the annular gap (0.25-mm thick) between the molybdenum cylinders with the aid of the associate capillary force. Completion of the casting is signaled by the appearance of molten material at the bleed hole. After the assembly cooled, the top and bottom (see Figure 22) were machined off and the center hole was made by electric discharge machining.

The three-inch-long cylinder is mounted in a bell jar and heated by electron bombardment. A photograph of a cast sapphire unit under test is shown in Figure 23. The outside temperature was 1650 K and the temperature difference across the cast sapphire layer was approximately 20 K (measured by an optical pyrometer) at a heat flux of about 40 W/cm^2. The outside of the unit was machined with a fine thread to increase its thermal emissivity.

The initial room temperature resistance was over 10^8 ohms. The initial resistance at operating temperature (i.e., 1650 K) was two ohms. After 100 hours of testing, the room temperature resistance had decreased to about 0.1 ohms and the operating temperature resistance was almost a dead short.

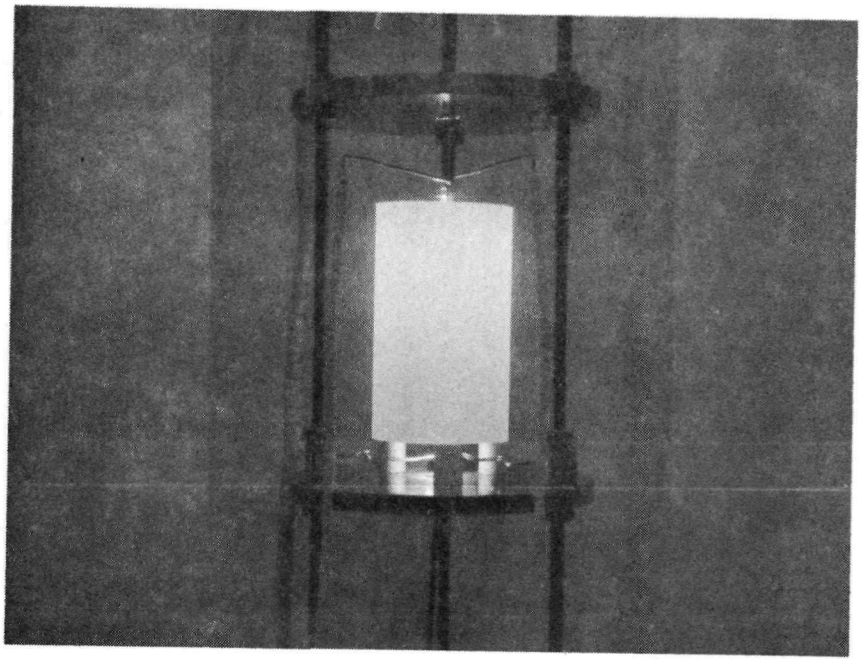

Figure 23 Cast Sapphire Assembly Under Test

After termination of the test, the unit was sectioned along the axis. Some cracks were evident, but were not in a direction to decrease heat or electrical flow.

Apparently, the failure was caused by carburization of the organic fluid that penetrated the radial cracks in the cast sapphire during the electrical discharge machining. There was also evidence of sapphire-molybdenum interaction that presumably took place during the casting operation.

A second assembly is being machined. It is intended that the casting will be performed only slightly above the melting point and that the ends will be sawed off.

B. Semiconductor Lead

In principle, the use of a "P" type thermoelectric (TE) lead in combination with a thermionic energy converter (TEC) would recover a larger fraction of the lead losses associated with a TEC so that the combined direct conversion efficiency is larger than with either thermionics or thermoelectrics, individually.

The analysis of a TEC using a "P" lead with hypothetical materials properties was given in Progress Report No. 35. These calculations have been refined using assumed thermoelectric property data supplied by Mr. Valvo Raag of Syncal Corporation. The effect of contact resistivity on terminal efficiency (for a one-cm-long TE lead) is shown in Figure 24 for barrier indicies of 1.9 and 2.0 eV. For the stated assumptions, the calculations show that contact resistivities up to 1000 $\mu\Omega-cm^2$ should not significantly degrade the lead efficiency. Typically, contact resistivities well below this value have been obtained with SiGe thermoelements. However, pressure contacts to PbTe thermoelements have often exceeded 1000 $\mu\Omega-cm^2$.

2.2.2 TASK XII. CORRELATION OF DESIGN INTERFACES

The objective of this task is to provide technical coordination between Thermo Electron and other contractors as well as with government agencies in order to assure overall compatibility of design, materials and interfaces between the thermionic conversion and other subsystems. This effort will be continuously updated.

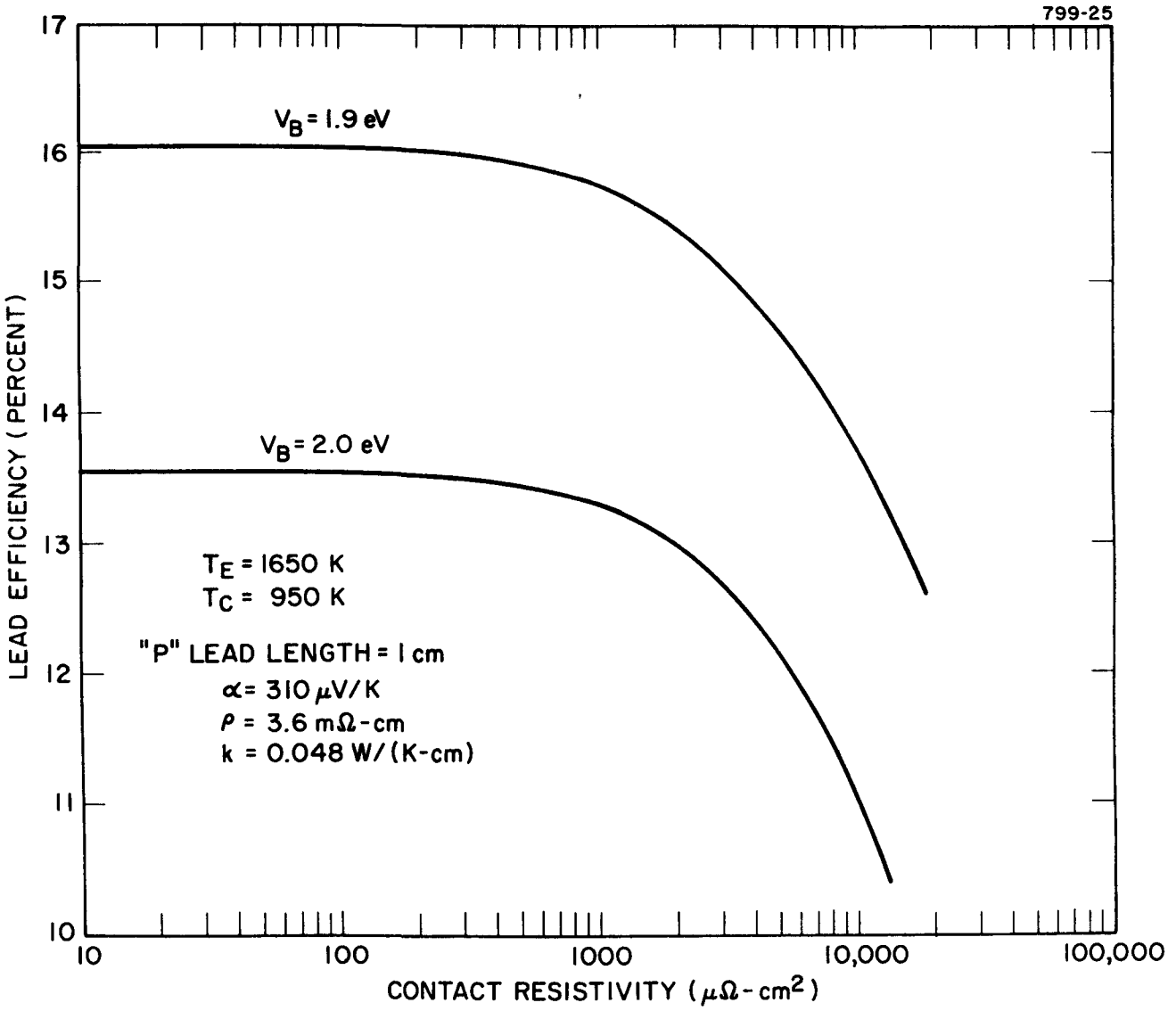

Figure 24. Calculated Terminal Efficiency of Thermionic Converter with "P" Lead as a Function of Contact Resistivity

A Nuclear Electric Propulsion Interface Working Group Meeting was held September 27 and 28 at JPL. F.N. Huffman and G. Miskolczy of Thermo Electron participated in the workshop. The design interface status prior to the workshop will be described below.

Each molybdenum-lithium reactor heat pipe is equipped with two thermionic converters. The nominal diameter of the emitter is 40 mm and the nominal length is 160 mm. The details of the converter design are described in Progress Report No. 39. An illustration of the thermionic reactor system is shown in Figure 25. The thermionic converters are arranged in four layers (A through D) and eight concentric rings (1 through 8). Details of the converter interconnections are shown in the radial section of the system (see Figure 26). The horizontal section is shown in Figure 27. Four converters are connected in parallel, arranged radially, and the parallel sets are connected in series with the busbars shown. The collector and emitter leads are at opposite ends of the thermionic converters. Adjacent rows of converters are reversed end-to-end to minimize the length of the interconnecting leads.

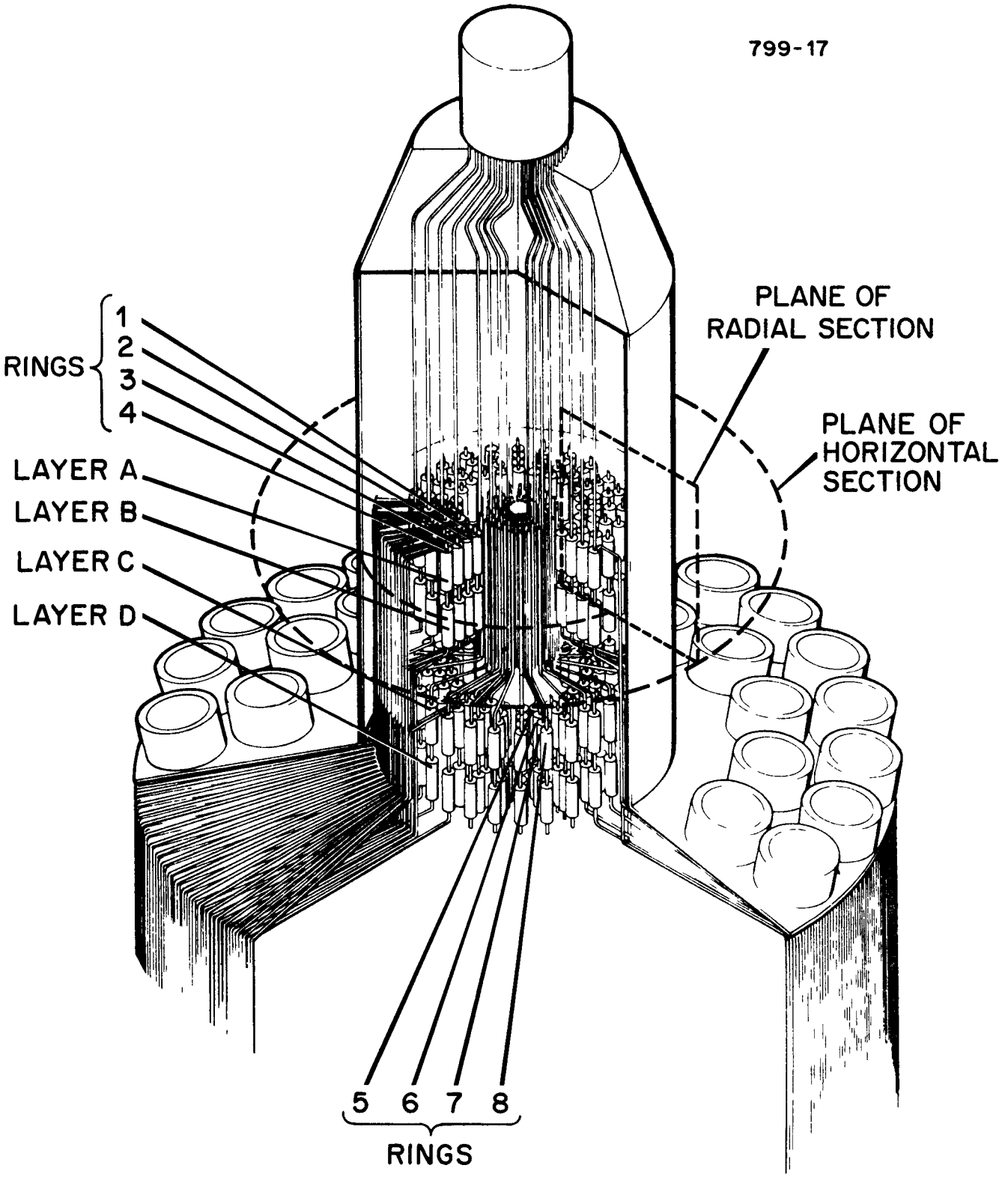

Figure 25. Illustration of Thermionic Reactor System

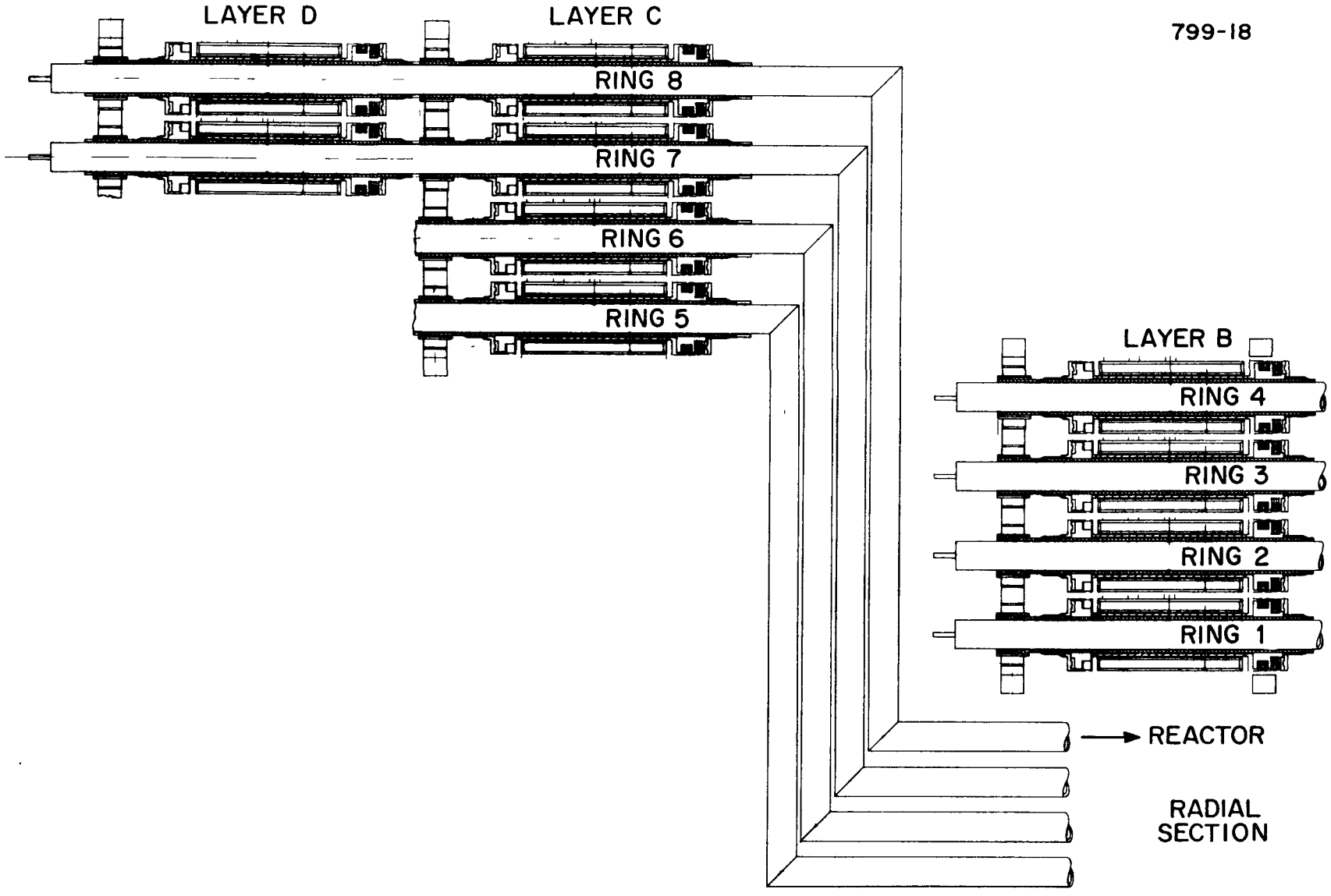

Figure 26. Radial Section of Thermionic Conversion System

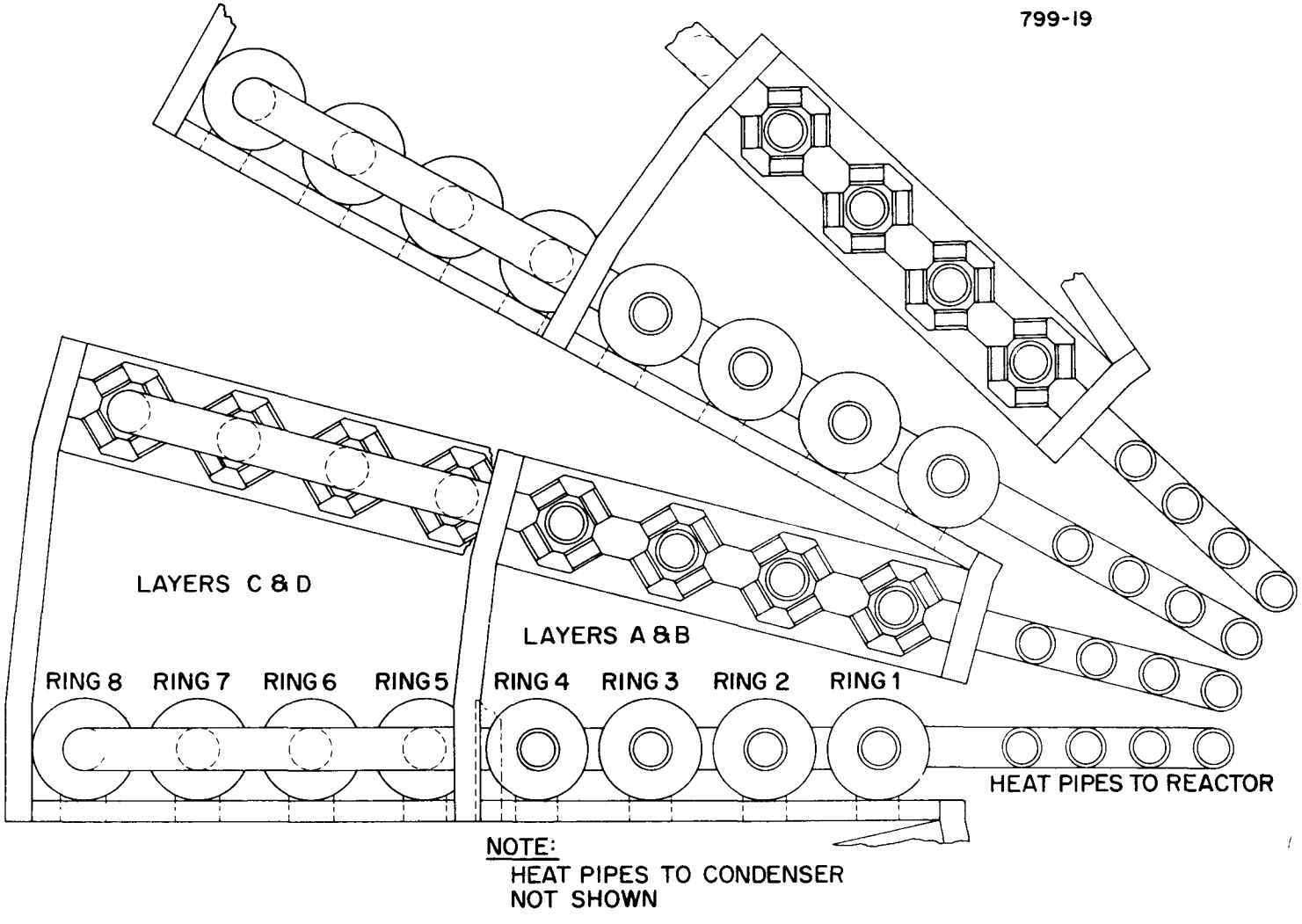

Figure 27. Horizontal Section of Thermionic Conversion System

An assembly sequence recommended by Thermo Electron is given in Table V. It is assumed that the emitter section of the reactor heat pipes is provided to Thermo Electron with the appropriate wick structure in place as shown in Figure 28. Then the emitter surface is assembled and the sapphire emitter insulator is cast in place. Subsequently, the emitter ends are ground to electrically separate the emitter into two sections, as illustrated in Figure 29. Next, the completed collector assemblies, including pretested collector heat pipes, are slipped over the emitter structure, as shown in Figure 30. Afterwards, the emitter sleeves are magnetically formed to the emitters and the joints are electron beam welded. This step is illustrated in Figure 31. At this point the converter is evacuated, degreased, and charged with cesium. During this procedure the emitters are heated by an electron bombardment filament, and collector cooling loops are attached (see Figure 32). The converter is completely processed and fully tested before assembly of the reactor heat pipe and the reactor. The completed converter assmembly is shown in Figure 33.

TABLE V

PROPOSED ASSEMBLY PROCEDURE

1. CONVERTER SECTION OF EMITTER HEAT PIPE (MOLY) PROVIDED BY LASL.
2. CAST SAPPHIRE BETWEEN HEAT PIPE AND EMITTER SUBSTRATE (MOLY).
3. ATTACH COLLECTOR SUBASSEMBLY (E.G., OXIDE COLLECTOR SURFACE ON NIOBIUM, TRILAYER, BELLOWS, SEAL, CESIUM-GRAPHITE RESERVOIR AND COLLECTOR HEAT PIPE).
4. BOND Mo-Re SLEEVE TO EMITTER WITH MAGNETIC PINCH.
5. OUTGAS, CHARGE AND TEST CONVERTERS (WITH EB).
6. EB CONVERTER SECTION TO REACTOR SECTION OF HEAT PIPE.
7. OUTGAS AND CHARGE HEAT PIPE WITH LITHIUM.
8. TEST EMITTER HEAT PIPE AND CONVERTER.
9. WELD RADIATOR PIPES ONTO CONVERTERS.
10. OUTGAS AND CHARGE RADIATOR HEAT PIPES.
11. TEST EMITTER HEAT PIPE/CONVERTER/COLLECTOR HEAT PIPE UNIT.
12. ASSEMBLE INTO REACTOR.
13. COUPLE TO BALANCE OF POWER SYSTEM.
14. INTEGRATE WITH SPACECRAFT.

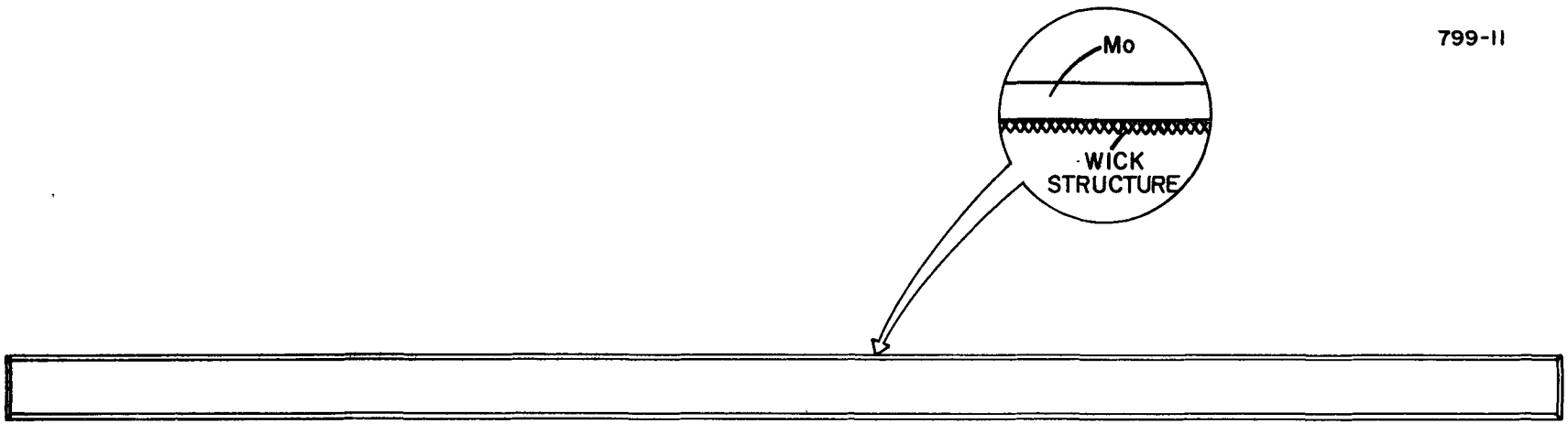

Figure 28. Emitter Heat Pipe

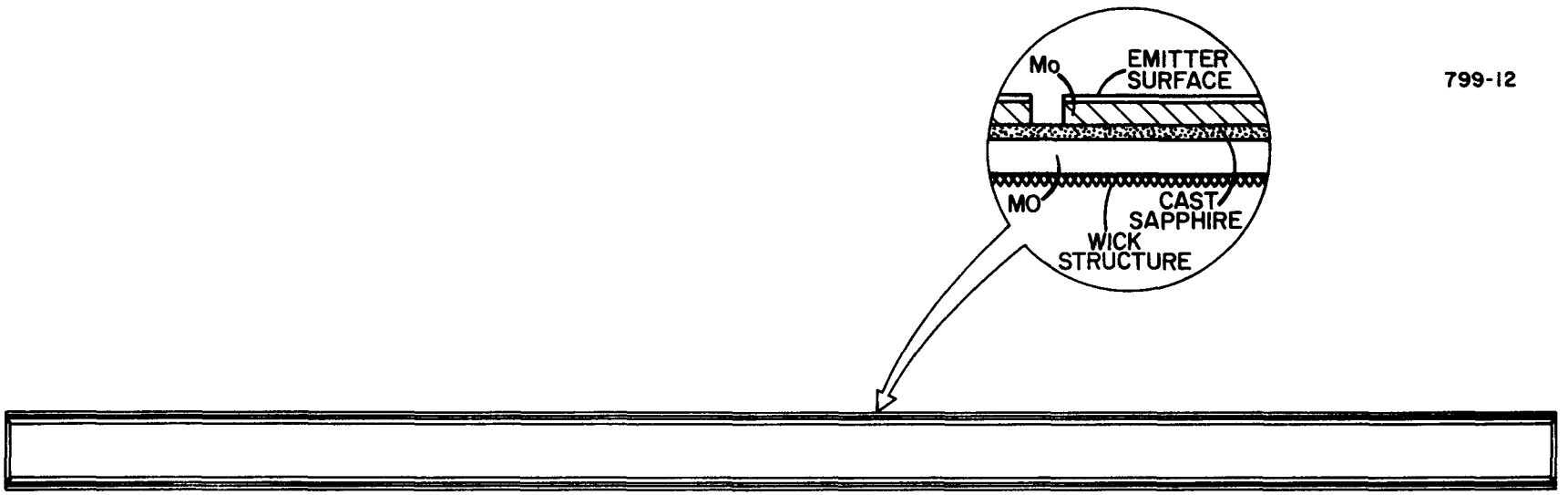

Figure 29. Emitter Heat Pipe with Emitter Surface Cast in Place

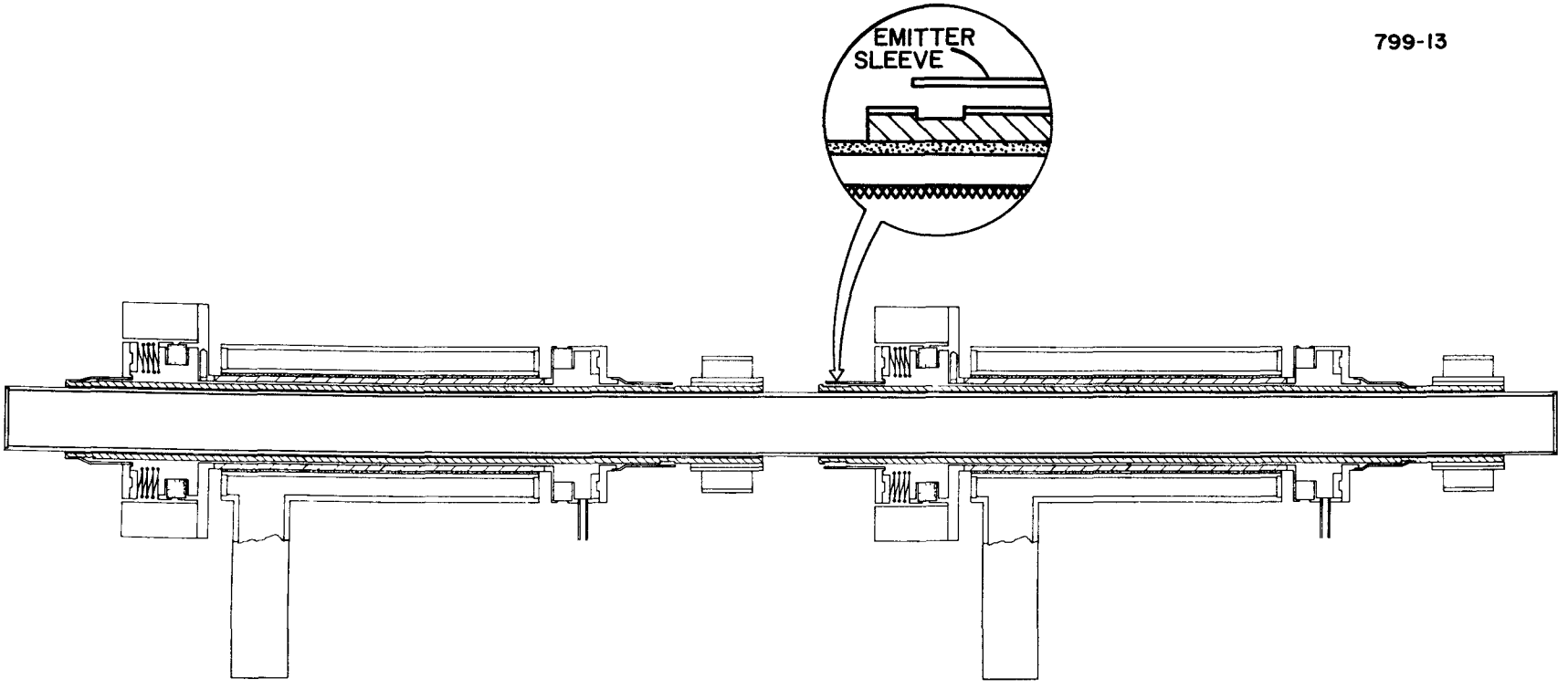

Figure 30. Emitter and Collector Assembled

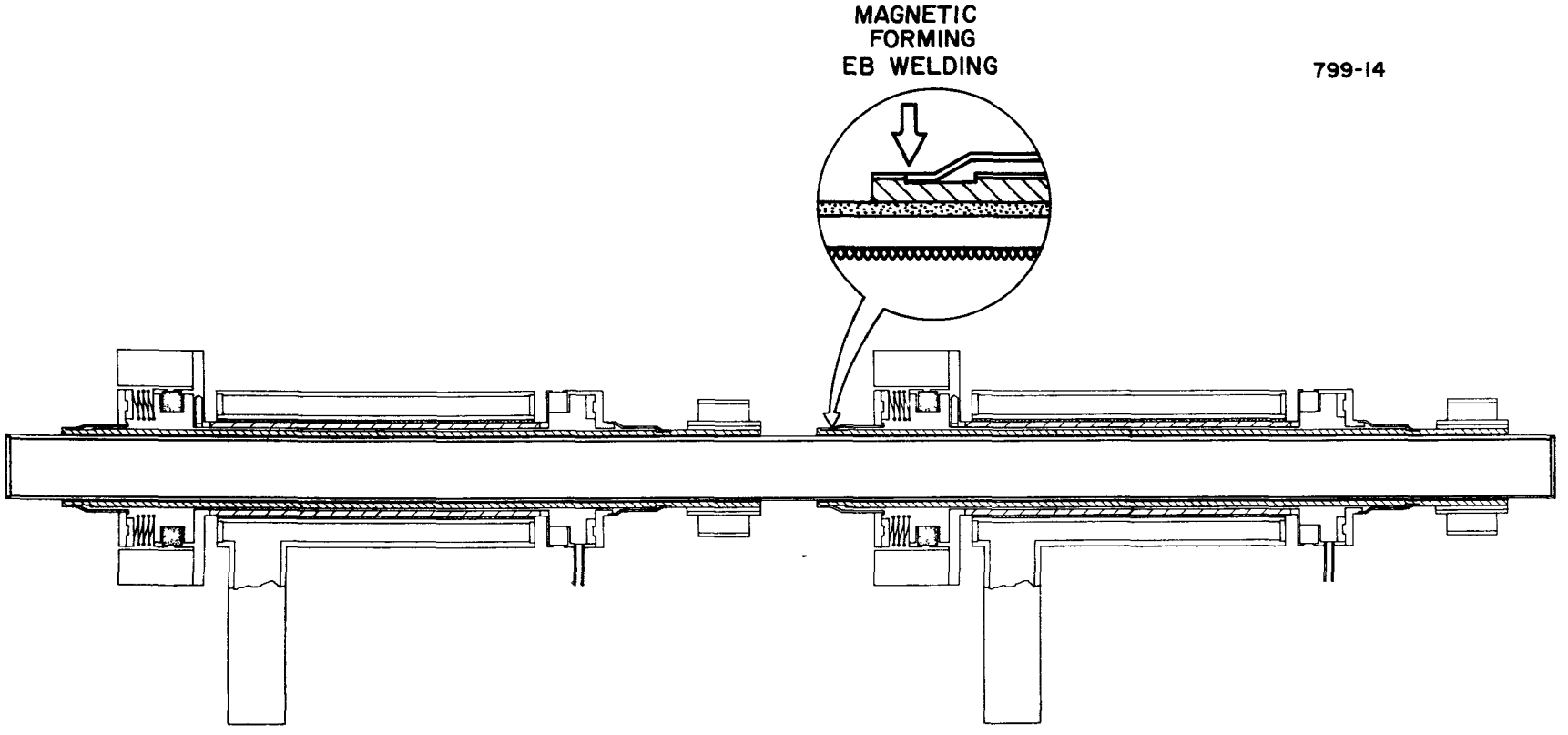

Figure 31. Magnetic Forming and Electron Beam Welding of Emitter Sleeve

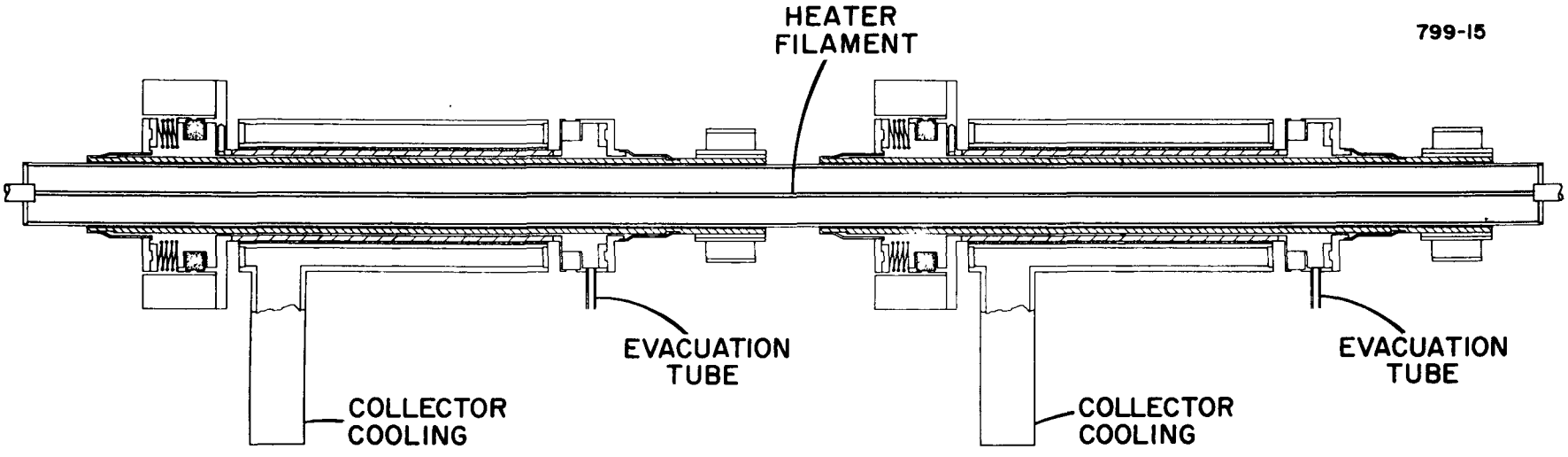

Figure 32. Converter Evacuation and Processing Using Electron Bombardment Heating

799-10

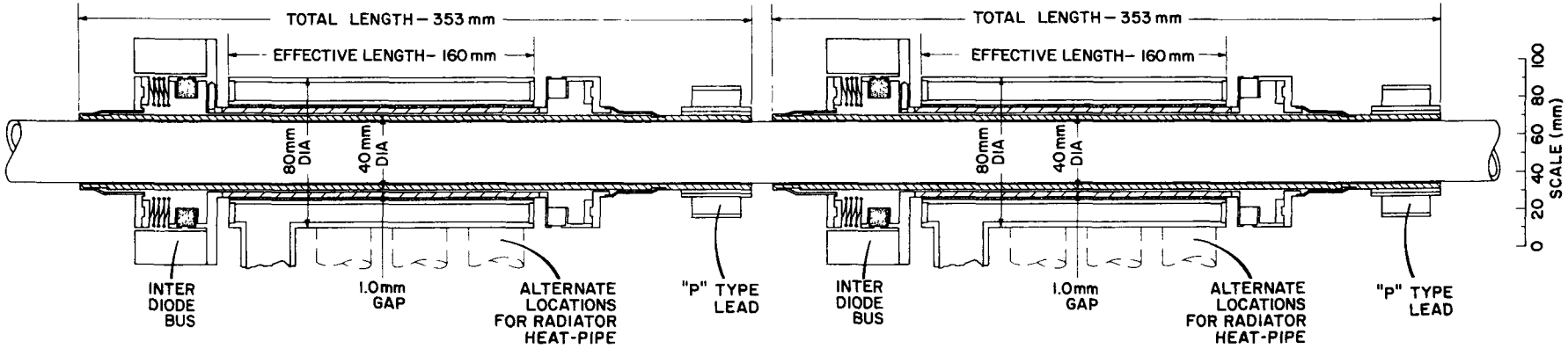

Figure 33. Coupled Thermionic Converter Assembly

REFERENCES

1. L.R. Danielson and L.W. Swanson, "High Temperature Coadsorption Study of Zirconium and Oxygen on the W(100) Crystal Face," Surface Science 88, p. 14 (1979).

2. L. Holland, Vacuum Deposition of Thin Films, Chapman and Hall Ltd., London (1966), p 152-6.

3. G. Hohler, Solid Surface Physics, Springer-Verlag, New York (1979).

4. H.R. Greim, "Plasma Spectroscopy," Chap. 13, McGraw Hill (1964).

5. J. Lawless and S. H. Lam, Thermionic Energy Conversion Research Analysis, 1977-1978 Annual Report COO-2533-8, Dept. of Mech. and Aerospace Engr., Princeton University (1978).

6. D.W. Norcross and P.M. Stone, J. Quant. Spect. Rad. Trem. 8 655 (1968).

7. F.G. Baksht, B. Moighes and V.A. Nemchinskii, Soviet Phys. Tech. Phys. 13 1401 (1969).

8. F. Huffman, Progress Report No. 38, Thermo Electron Report No. TE 4258/4247-135-79, (1979).

9. M. Fabry and J.R. Cussenot, J. Appl. Phys. 43 357 (1972).

10. D.E. Moe, Phys. Rev. 104 694 (1956).

11. D.R. Bates and Griffin, Proc. Phys. Soc. (London) A68 90 (1955).

12. H.W. Drawin, Z. Phys. 211 404 (1968).

13. H.W. Drawin, Z. Phys. 225 483 (1969).

14. C. Lee, "Topical Report, Investigations of a Pulsed Triode Converter with Guard Collector," Thermo Electron Report No. TE4247-219-79, (1979).

APPENDIX

DOUBLE SHEATH FORMATION

GLOSSARY OF SYMBOLS

a	Dimensionless Ion Cut-Off Energy
c	Dimensionless Electron Temperature
f_e	Electron Distribution Function
f_i	Ion Distribution Function
J_s	Current Density
J	Richardson Current Density
j	Dimensionless Current Density
k	Boltzmann Constant
m	Electron Mass
M	Ion Mass
$N_e(0)$	Density of Emitter Electron
$N_e(p)$	Density of Half-Maxwellian Distribution Electron From Plasma
$N_i(p)$	Density of Half-Maxwellian Distribution Ion From Plasma
n_e	Electron Density
n_i	Ion Density

GLOSSARY OF SYMBOLS (Continued)

n_{plasma}	Plasma Charged Particle Density
v	Velocity of Charged Particles
V_c	Electrostatic Potential
V	Cutoff Energy of Half-Maxwellian Distribution Ions
ψ	Dimensionless Potential
ψ_p	Dimensionless Plasma Potential
ρ_e	Dimensionless Electron Density
ρ_i	Dimensionless Ion Density

APPENDIX

DOUBLE SHEATH FORMATION

1. BACKGROUND

The I-V characteristics of cesium thermionic diodes operating in the ignited mode near optimum power show a knee. When the converter is operating in the region above the knee, the dominant contributor to the arc drop is the difference of the sheath heights (i.e., the potential difference in the plasma is either very small or makes a contribution to reduce the arc drop). The increase in output current is usually not able to compensate for the loss of output voltage. For this reason, the shape of the I-V characteristic below the knee is different from that above the knee. The location of the knee is a good indicator of the maximum power and the maximum efficiency points. Under fully optimized conditions, the knee also indicates the barrier index of the converter. Therefore, how and where the knee will apprear is of great theoretical and practical interest. Some workers in the thermionic field have speculated that the appearance of the knee is due to the formation of the double sheath. This study evaluates this hypothesis.

2. ASSUMPTIONS

The problem of the space charge in the sheath is considered for the case when electrons with a half-Maxwellian distribution are introduced into the sheath at the electrode and plasma-sheath boundary and the ions are introduced into the sheath from the plasma-sheath boundary with a cutoff half-Maxwellian distribution. The inelastic and short range binary elastic collisions are neglected, but each charged particle interacts with the Coulomb field of all other charged particles. These assumptions allow for exact calculation of the self-consistent space charge potential distribution. The match between the sheath and the plasma is based on the continuities of potential, current and charged particle densities. These values are obtained independently from the sheath and the plasma calculations.

3. DENSITY FUNCTIONS OF CHARGED PARTICLES

The one-dimensional collisonless Boltzmann equations for the charged particles with external force replaced by the gradient of electrostatic potential with appropriate signs are:

$$u \frac{\partial f_e}{\partial x} + \frac{e}{m} \frac{dV}{dx} \frac{\partial f_e}{\partial u} = 0 \qquad (1)$$

$$u \frac{\partial f_i}{\partial x} - \frac{e}{M} \frac{dV}{dx} \frac{\partial f_i}{\partial u} = 0 \tag{2}$$

where f_e and f_i are electron and ion distribution functions, u is the velocity of the charged particles, V is the electrostatic potential, m and M are the masses of the electron and ion, respectively. The distribution functions f_e and f_i are subjected to the boundary conditions that the particles are introduced into the sheath with half-Maxwellian or cut-off half-Maxwellian distributions. The solution satisfying these assumptions are in the form of

$$f_e (V, u) = 2 N_e \left(\frac{m}{2\pi kT_e}\right)^{\frac{1}{2}} \exp\left[-\frac{m}{2 kT_e}\left(u^2 - \frac{2 eV}{m}\right)\right] \tag{3}$$

$$f_i (V, u) = 2 N_i \left(\frac{M}{2\pi kT_i}\right)^{\frac{1}{2}} \exp\left[-\frac{M}{2 kT_i}\left(u^2 - \frac{2 e (V + V_c)}{M}\right)\right] \tag{4}$$

where N is the density of the charged particles at the boundary, T is the temperature and V_e is the cutoff energy of ion.

It will be convenient to introduce the dimensionless variables

$$\psi = \frac{eV}{kT_E} \tag{5}$$

$$n = \frac{\int_{-\infty}^{\infty} f (V, u)\, du}{N_e (0)} \tag{6}$$

where T_E is the electrode temperature, k the Boltzmann constant, and $N_e(0)$ is the density of the emitted electrons from the electrode. With these new variables and for a monotonic accelerating field, the density functions of electrons and ions in the sheath can be formulated as:

$$n_e(\psi) = H(\psi) + \frac{N_e(p)}{N_e(0)} e^{c(\psi - \psi_p)} \left[1 + E(c\psi)\right] \tag{7}$$

$$n_i(\psi) = \frac{N_i(p)}{N_e(0)} \frac{H(\psi_p + a - \psi)}{H(a)} \tag{8}$$

$$a = \frac{e V_c}{kT_E}, \quad \psi_p = \frac{e V_p}{kT_E}$$

$$E(x) = \frac{2}{\sqrt{\pi}} \int_0^{x^{\frac{1}{2}}} e^{-t^2} dt \tag{9}$$

$$H(x) = e^x \left[1 - E(x)\right] \tag{10}$$

$N_e(p)$ and $N_i(p)$ are the electron and ion densities at the plasma-sheath boundary due to the introduction of charged particles from the plasma. The dimensionless sheath height is given by ψ_p, a is the dimensionless cutoff energy of the ions and c is the

ratio between electron and ion temperatures. With these distribution functions, the current density, J, across the sheath can be expressed as:

$$J = J_s \left[1 - \frac{N_e(p)}{N_e(0)} \left(\frac{T_e}{T_E} \right)^{\frac{1}{2}} e^{-c\psi_p} + \frac{N_i(p)}{N_e(0)} \left(\frac{m}{M} \right)^{\frac{1}{2}} / H(a) \right] \tag{11}$$

where J_S is the Richardson current by the electrode. Further defining:

$$j = J/J_s$$

$$\rho_e = \frac{N_e(p)}{N_e(0)} \tag{12}$$

$$\rho_i = \frac{N_i(p)}{N_i(0)}$$

one obtains:

$$n_e(\psi) = H(\psi) + \rho_e e^{c(\psi - \psi_p)} \left[1 + E(c\psi) \right] \tag{13}$$

$$n_i(\psi) = \rho_i H(\psi_p + a - \psi)/H(a) \tag{14}$$

$$j = 1 - \rho_e/\sqrt{c} \exp(c\psi_p) + \rho_i \left(\frac{m}{M} \right)^{\frac{1}{2}} / H(a) \tag{15}$$

As a result of the collisional energy exchange between ions and atoms, the ion temperature, T_i, may be assumed to be equal to the atomic temperature, T_a. In the region near to the electrode, T_a equals the temperature of the electrode, T_E. Therefore, T_i may be assumed to be equal to T_E at this location.

4. BOUNDARY CONDITIONS

a. Quasi-Neutrality is generally assumed for the plasma. Therefore, at the boundary between the sheath and plasma:

$$n_{plasma} = n_i(\psi_p) = n_e(\psi_p) \tag{16}$$

This gives:

$$\rho_i = n_{plasma}/N_e(0) \tag{17}$$

$$\rho_e = \left[\rho_i - H(\psi_p)\right] / \left[1 + E(c\psi_p)\right] \tag{18}$$

Substituting the above expressions into Equation (15), one obtains:

$$j = 1 - \rho_i \left\{ \left[1 + E(c\psi_p)\right]^{-1} - \left(\frac{m}{M}\right)^{\frac{1}{2}} / H(a) \right\} + \frac{H(\psi_p)}{\sqrt{c}\, \exp(c\psi_p) \left[1 + E(c\psi_p)\right]} \tag{19}$$

b. A sheath boundary condition first used by Allen and Thonemann[1] has later been derived by Andrew and Allen,[2] namely,

$$\frac{dn\ (\psi)}{d\psi} = 0 \quad \text{at} \quad \psi = \psi_p \tag{20}$$

This condition gives:

$$\frac{d\ n_e\ (\psi)}{d\psi} = \frac{d\ n_i\ (\psi)}{d\psi} \quad \text{at} \quad \psi = \psi_p \tag{21}$$

Using Equations (13) and (14), one has:

$$\rho_i \left[\frac{1}{\sqrt{\pi a}\ H\ (a)} - 1 \right] - c\rho_e \left[1 + E\ (c\psi_p) + \frac{e^{-c\psi_p}}{\sqrt{c\pi\ \psi_p}} \right] - H\ (\psi_p) + \frac{1}{\sqrt{\pi\ \psi_p}} = 0 \tag{22}$$

c. It is usually assumed that the gradient of the potential vanishes at the plasma-sheath boundary. At the moment the double sheath is starting to form, the gradient of potential also vanishes at the electrode boundary. Poisson's equation states that:

$$\frac{d^2\psi}{dx^2} = 4\pi\ n\ (x) \tag{23}$$

$$\int \frac{d^2\psi}{dx^2} \cdot \frac{d\psi}{dx} \cdot dx = 4\pi \int n\ (x)\ \frac{d\psi}{dx}\ dx$$

$$\frac{1}{2}\left(E_1^{\,2} - E_2^{\,2} \right) = 4\pi \int_{\psi_2}^{\psi_1} n\ (\psi)\ d\psi \tag{24}$$

Since E vanishes at both boundaries, the integral must be zero. That is,

$$\int_{\psi_2}^{\psi_1} n\,(\psi)\, d\psi = 0 \tag{25}$$

which imples:

$$\int_{o}^{\psi_p} \left[n_e\,(\psi) - n_i\,(\psi) \right] d\psi = 0 \tag{26}$$

Substituting Equations (13) and (14) into the above equation and carrying out the integration, one obtains.

$$G\,(\psi_p) - 1 + \frac{\rho_e}{c}\, e^{-c\psi_p} \left[L\,(c\psi_p) - 1 \right] + \frac{\rho_i \left[G\,(a) - G\,(\psi_p + a) \right]}{H(a)} = 0 \tag{27}$$

where

$$G\,(x) = e^{x} \left[1 - E\,(x) \right] + 2\sqrt{\frac{\pi}{x}} \tag{28}$$

$$L\,(x) = e^{x} \left[1 + E\,(x) \right] - 2\sqrt{\frac{\pi}{x}} \tag{29}$$

5. SOLUTIONS AND RESULTS

With c and a held as constants, the relation among j, ψ_i and ρ_i can be obtained from Equation (19) and they are plotted in Figure A-1. The current that flows through the sheath and across the plasma must be the same. j is a common variable. Besides potential,

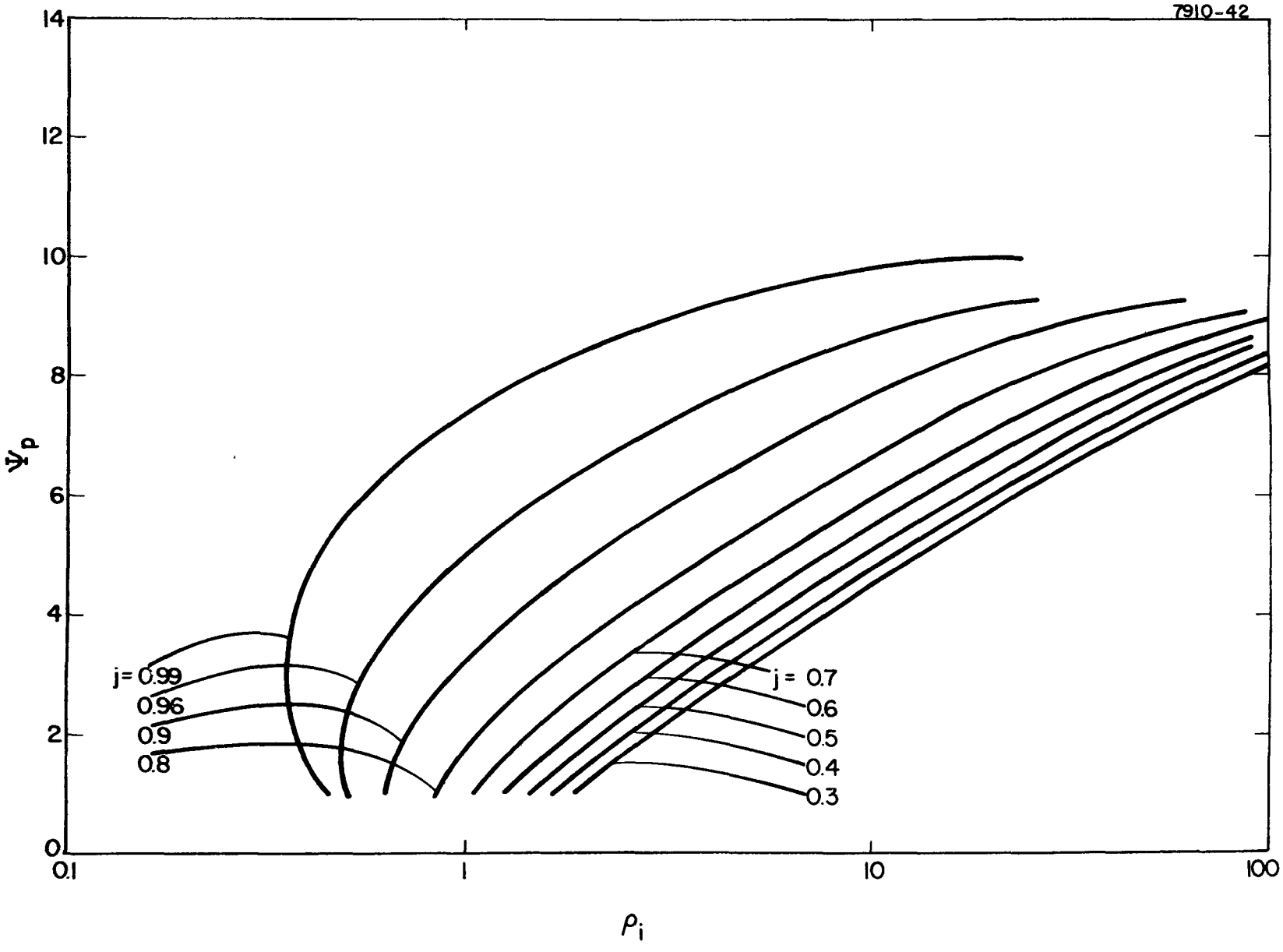

Figure A-1. Relation Between ψ_ρ and ρ_i as Function of j

ψ_p, and plasma density, N_p, there are other conditions to limit the amount of current that can flow through the sheath and the plasma. The flexibility in the values of ψ_p and ρ_i for the same amount of current gives the possibility that the sheath and the plasma can be matched at their interface. Because of the ratio of the masses between electron and ion, the contribution of the ion current to the total current is small. The value of cutoff energy affects only the ion current, therefore, the relation among j, ψ_p, and ρ_i is not sensitive to the value of a. The value of c affects the electron current from the plasma toward the electrode. Electron current is the main component of the total current; therefore, the value of c has a profound effect to the relation among j, ψ_p and ρ_i. This effect is shown in Figure A-2. For example, with the same values of ψ_p and ρ_i, a normalized current, j, of 0.3 or 0.8 can be flowed through the sheath depending on the value of c.

Boundary conditions (b) and (c) are the additonal conditions to be satisfied in the sheath. Condition (b) is general for any form of sheath. Condition (c) holds just as the sheath is starting to become double valued.

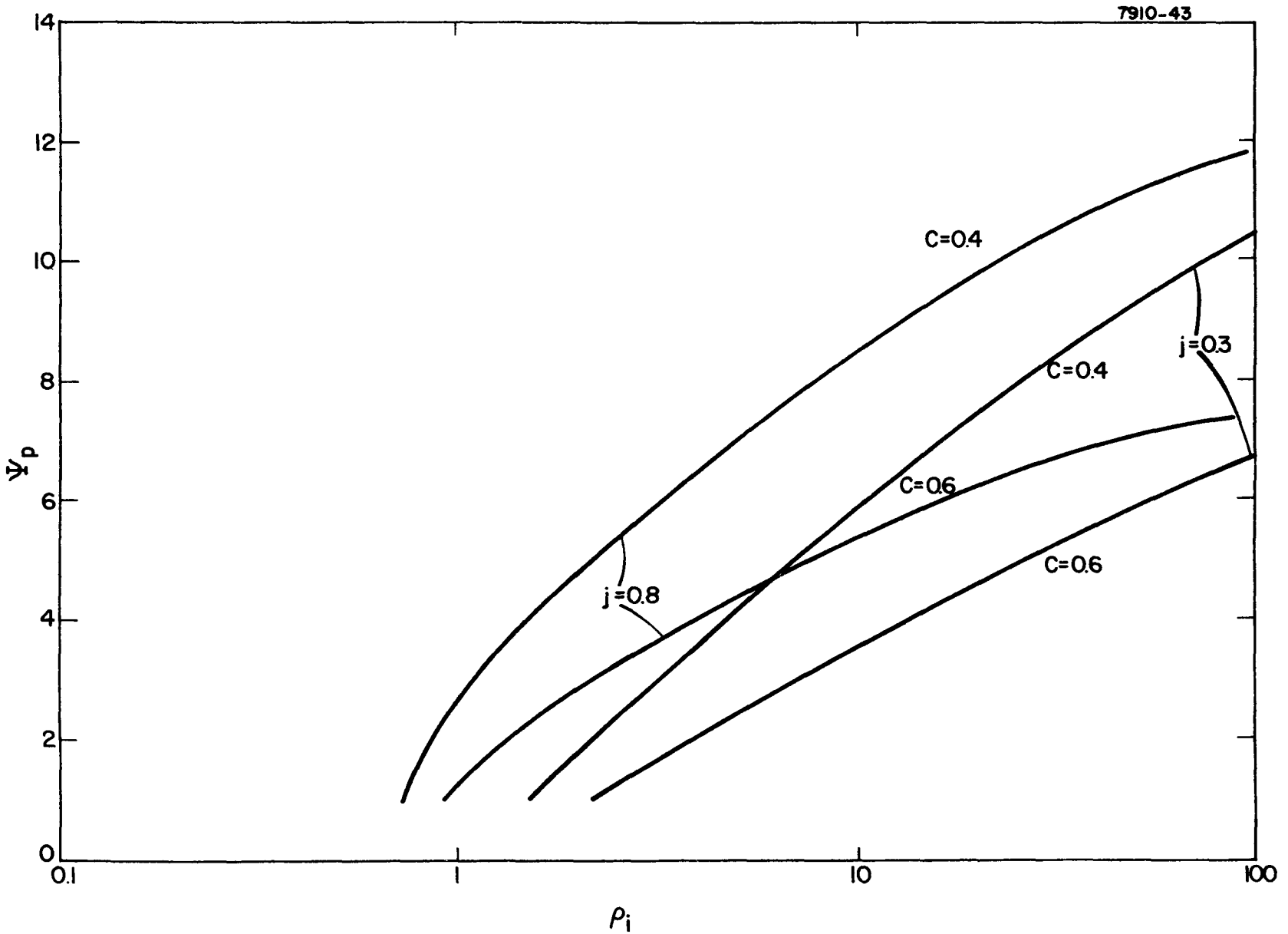

Figure A-2. Effects of (c) and the Relation of ψ_ρ and ρ_i

The relation between ψ_p and ρ_i can be obtained by solving Equations (22) and (27). The results are plotted in Figure A-3. The results are not sensitive to the values of c or a. For a fixed value of c, the value of a is almost constant. The most important result indicated by these curves is that the double sheath can only be formed with the value of ρ_i less than 1.7 (ρ_i is the ratio between the plasma density and the electron density corresponding to saturation current density). To limit the value of ρ_i to be less than 1.7 rules out the possibility of forming a double sheath on the collector side of the thermionic converter.

On substituting the foregoing results into Equation (19), one obtains the relation between j and ψ_p . These relations are plotted in Figure A-4. The results for two sample plasma calculations are also plotted in this figure. The intersection of plasma and sheath solutions indicates the matching conditions between the sheath and the plasma. Based on the results of plasma calculations, the value of $c \sim 6$ for typical thermionic converter conditions. For case (1), the double sheath is formed at $j \sim 0.48$ and $\psi_p \sim 0.9$ while for case (2) $j \sim 0.44$ and $\psi_p \sim 0.8$.

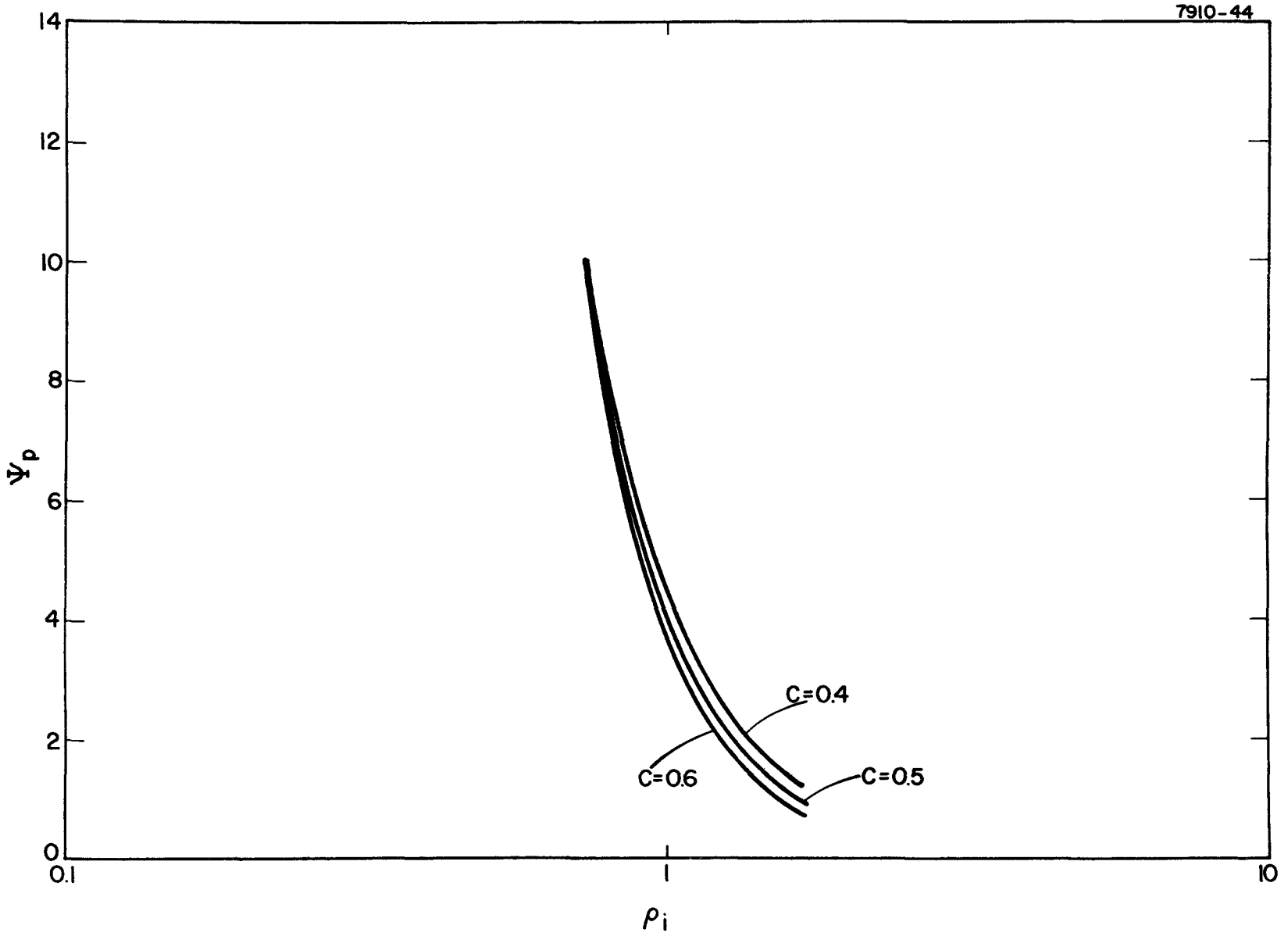

Figure A-3. Condition of the Function of Double Sheath

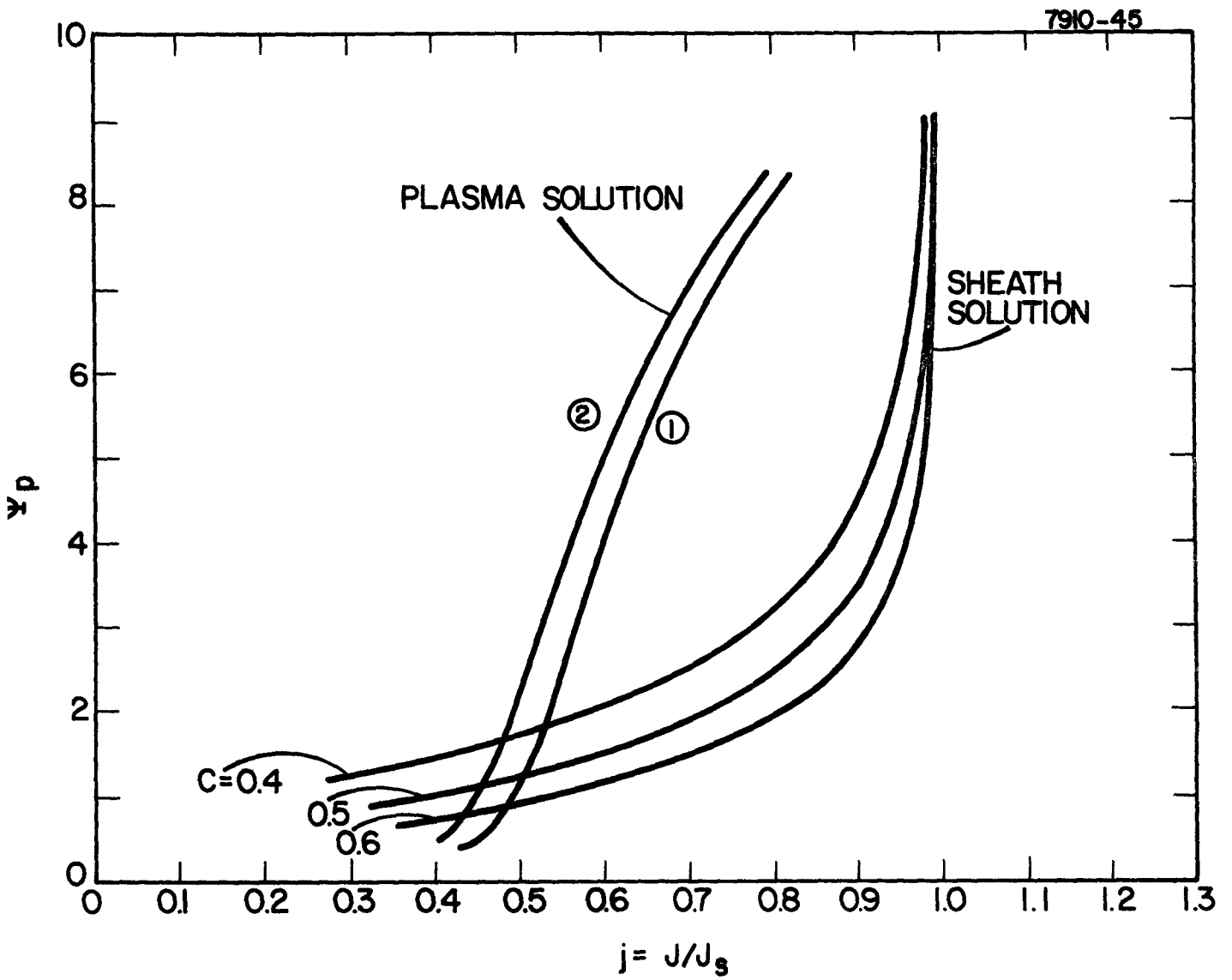

Figure A-4. With ψ_ρ and j as Matching Parameters to Identify the Matching Condition of the Sheath and the Plasma for the Formation of Double Sheath

The results shown in Figures A-1 and A-2 and the results for the same sample plasma conditions are combined in Figures A-5 and A-6. On Figure A-5 shows that the results of the sheath calculation intersects that of the plasma calculation at $\psi_p = 1$ and $P_i = 1.55$. The values of the currents for the plasma calculation are indicated on the plasma curve. At the intersection, j equals 0.48. The expression of j from Equation (19) is plotted as the dashed curve. The intersection of the dashed curve and the sheath solutions is not exactly the same as the intersection of the plasma solution and the sheath solution. This slight discrepancy indicates that the match is not perfect. However, if we consider all assumptions that have been used in the sheath and the plasma region, this slight discrepancy can be tolerated. The matching conditions for another case are given in Figure A-6. This discrepancy is also quite small.

The I-V characteristics for the plasma calculations are given in Figure A-7. The matching conditions for the formation of the double sheath are indicated on the curves. They show that the formation of the double sheath is below the appearance of the knee.

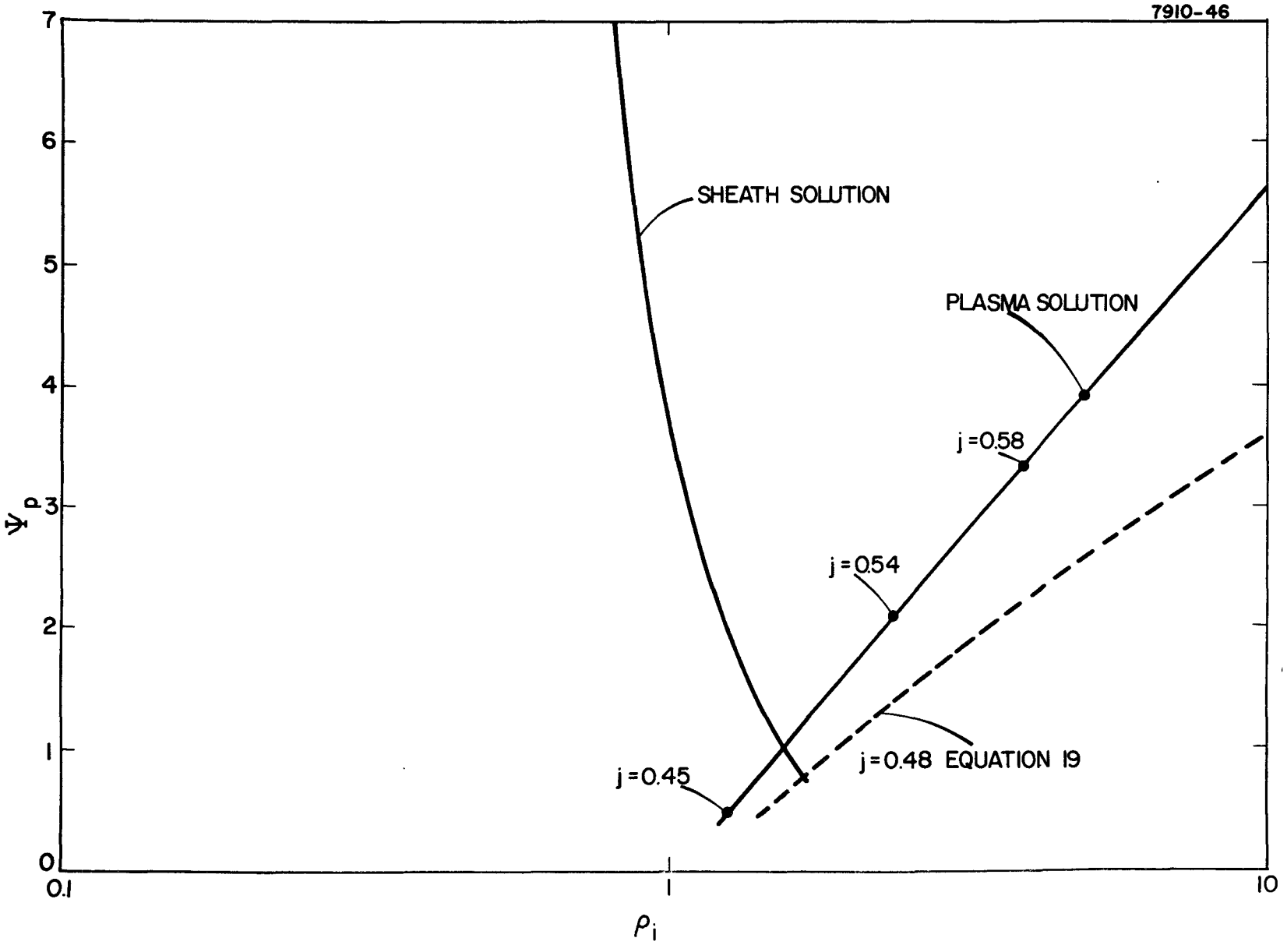

Figure A-5. With ψ_ρ and ρ_i as the Matching Parameters to Identify the Matching Condition of the Sheath and the Plasma for the Formation of the Double Sheath

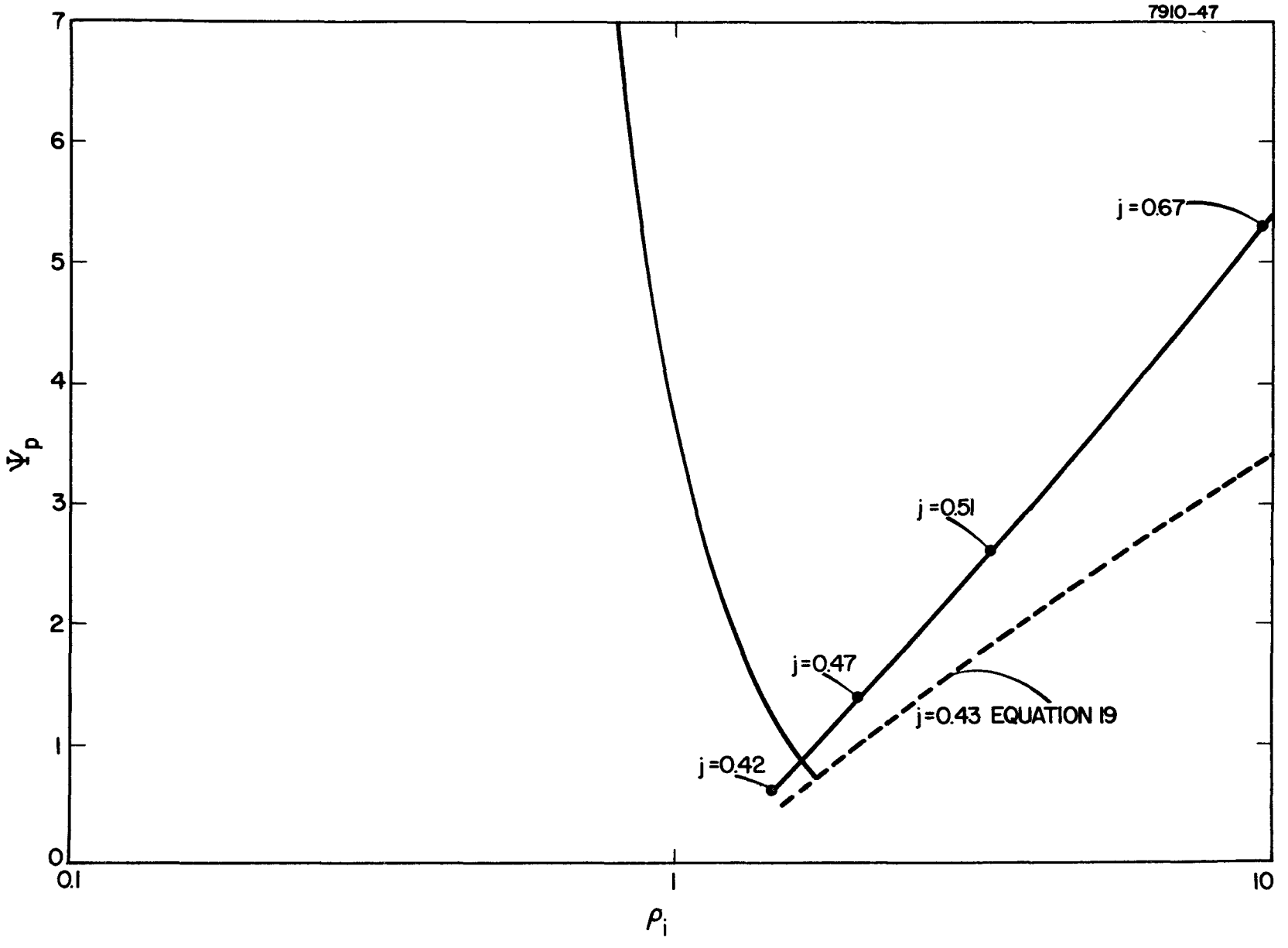

Figure A-6. With ψ_ρ and ρ_i as the Matching Parameters to Identify the Matching Condition Between the Sheath and the Plasma for the Formation of Double Sheath

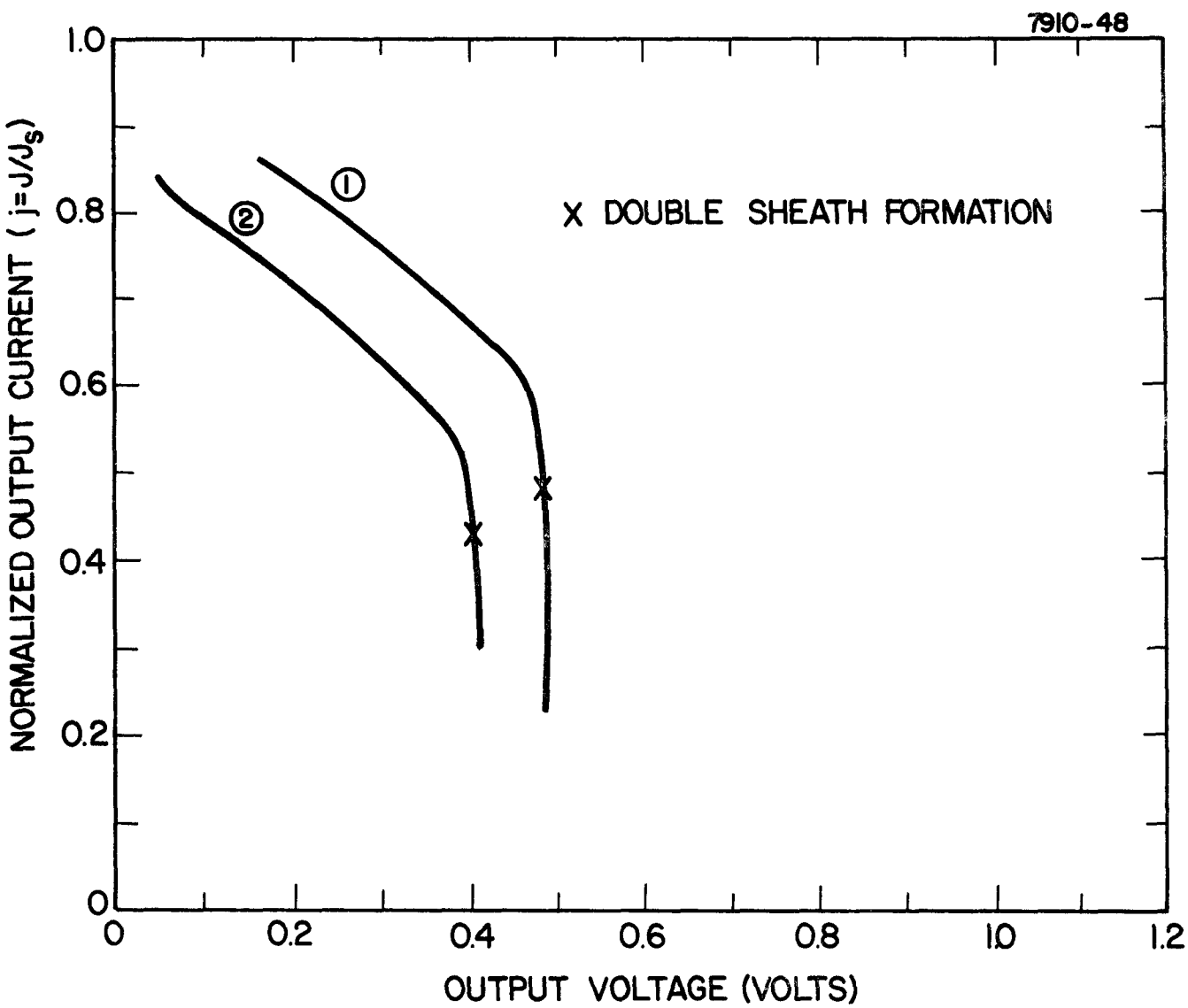

Figure A-7. I-V Characteristics of Plasma Calculations

6. CONCLUSION

The following conclusions can be drawn from this analysis:

(1) The formation of the double sheath and the match between the sheath and the plasma is predicted by the theory presented herein.

(2) The double sheath will be formed for the constraint of ρ_i 1.7. This constraint rules out the possibility of the formation of double sheath on the collector side of the plasma.

(3) The double sheath is formed below the knee of I-V characteristic.

REFERENCES FOR APPENDIX

1. J.E. Allen, and P.C. Thonemann, 1954 Proc. Phys. Soc. B67, 768.

2. J.G. Andrew and J.E. Allen, 1971 Proc. R. Soc. London, A320, 459.